# BLACK BOX MODELING OF PASSIVE SYSTEMS BY RATIONAL FUNCTION APPROXIMATION

BY

RONG GAO

B.E., Northwestern Polytechnical University, 1995
M.S., Northwestern Polytechnical University, 1998

DISSERTATION

Submitted in partial fulfillment of the requirements
for the degree of Doctor of Philosophy in Electrical Engineering
in the Graduate College of the
University of Illinois at Urbana-Champaign, 2005

Urbana, Illinois

BLACK BOX MODELING OF PASSIVE SYSTEMS BY RATIONAL FUNCTION APPROXIMATION

Rong Gao, Ph.D.
Department of Electrical and Computer Engineering
University of Illinois at Urbana-Champaign, 2005
Jose E. Schutt-Ainé, Adviser

As the operation frequency of integrated circuit chips increases, electromagnetic effects of interconnect and packaging structures are no longer negligible and have to be accurately modeled and incorporated into the simulation, which is a challenging issue when simulation speed and accuracy are both required for facilitating the integrated circuit design.

Electromagnetic effects of a passive system can be characterized by measurements or full-wave simulations in the frequency domain. The results are expressed either in the form of input-output responses of a multiport network with a large number of sampled data in frequency domain or in the form of a high-order state-space model. Neither form is compact enough to be incorporated into circuit simulation directly. Various model-order reduction approaches have been developed to generate lower-order macromodels for the latter case, but are not applicable for the former case where a state-space expression is not available.

An efficient black-box modeling approach is proposed to construct rational function macromodels from sampled frequency-domain system responses. Orthogonal polynomials are employed to overcome the ill-conditioning problem associated with the curve fitting procedure. The performance of different polynomials is investigated and compared. Causality and stability of the macromodel are ensured inherently by the proposed method. Passivity enforcement is also discussed.

The modified minimum phase, all pass, and delay (MAD) method for black-box modeling is proposed and validated. Using this method, a black-box system is modeled as three parts, a minimum phase subsystem, an all-pass subsystem, and a delay term. Since this model precisely capture the physical characteristics of complicated networks in a wide frequency range, it significantly improves both the modeling efficiency and accuracy compared to existing rational function approximation methods.

# ABSTRACT

As the operation frequency of integrated circuit chips increases, electromagnetic effects of interconnect and packaging structures are no longer negligible and have to be accurately modeled and incorporated into the circuit simulation, which is a challenging issue when simulation speed and accuracy are both required for facilitating the integrated circuit design.

Electromagnetic effects of a passive system can be characterized by measurements or full-wave simulations in the frequency domain. The results are usually expressed in the form of input-output responses of a multiport network with a large number of sampled data. The tabulated data cannot be incorporated into circuit simulation directly.

An efficient black-box modeling approach is proposed to construct rational function macromodels from sampled frequency-domain system responses. Orthogonal polynomials are employed to overcome the ill-conditioning problem associated with the curve fitting procedure. The performance of different polynomials is investigated and compared. Causality and stability of the macromodel are ensured inherently by the proposed method. Passivity enforcement is also discussed.

The modified minimum phase, all pass, and delay (MAD) method for black-box modeling is proposed and validated. Using this method, a black-box system is modeled as three parts, a minimum phase subsystem, an all-pass subsystem, and a delay term. Since this model precisely capture the physical characteristics of complicated networks in a wide frequency range, it significantly improves both the modeling efficiency and accuracy compared to existing rational function approximation methods.

To Yunhui, with all my love

# ACKNOWLEDGMENTS

First and foremost, I would like to thank my adviser, Professor Jose E. Schutt-Ainé. Completion of this thesis would not have been possible without his continuous support and skillful guidance. I am also grateful for all his patience and encouragement for all the ups and downs during these four years of my study.

I thank my committee members, Professor Naresh Shanbhag, Professor Martin Wong, Professor Yun Chiu, and Professor Andreas Cangellaris, for their valuable time and suggestions. I would also like to thank Professor Gordon Kraft, Professor W. Thomas Miller, Professor Kondagunta Sivaprasad, Professor Kent Chamberlin, and Professor Michael Carter for all their support and help while I was at the University of New Hampshire.

My thanks to Wendem Beyene at Rambus and Yidnek Mekonnen in our group for the valuable discussions and suggestions, and for their continual willingness to spend time with me for this research.

I also thank all my friends at this campus and across the country for their friendship and for the joyful moments we shared.

Thanks to my big happy family, my parents, my sisters and brother, my parents-in-law, my aunt and uncle, and my cousin for all the consistent support, love, and encouragement all these years.

Finally, my deepest thanks go to my husband, Yunhui. This work would not have been completed without his love, support, patience, and encouragment. I am also grateful for his proofreading of this thesis.

# TABLE OF CONTENTS

# 1 INTRODUCTION

The topic investigated in this work is the efficient macromodel construction for complex systems, particularly passive systems.

This research is motivated by the increasing demand for accurate and efficient modeling of complex interconnect and packaging structures, which is a critical issue for signal integrity analysis in integrated circuit (IC) chip design, especially the state-of-the-art system-on-chip (SoC) and system-in-package (SiP) techniques.

As the operation frequency of today's IC chips increases, the electromagnetic effects become so significant that they can no longer be ignored or even coarsely approximated. They have to be accurately modeled and incorporated into the chip simulation. Otherwise, the chip simulation results cannot be accurate enough to guide or validate the design process.

The challenging issue here is how to incorporate the prohibiting complexity of electromagnetic effects into circuit simulation, where speed and accuracy are both necessary to facilitate the design process. Most interconnect and packaging structures have complicated three-dimensional (3D) geometries. Accurate characterization of these structures requires either measurement or full-wave electromagnetic simulations. The characterization results are usually expressed in three forms: (a) frequency domain response of the system in the form of tabulated data, (b) an equivalent circuit network, or (c) a matrix system constructed by discretizing either the differential or integral form of Maxwell's equation.

None of these forms of results can be readily incorporated into circuit simulation directly for practical applications. Method (a) involves a large number of sampling points. A direct Fourier transform for frequency-domain data or convolution for time-domain data are both too time-consuming to be applicable. Even the fast Fourier transform cannot satisfy the speed demand for computer-aided design simulators. Method (b) can be obtained by either the partial element equivalent circuit (PEEC) method [1], transmission line models, or other heuristic modeling approaches. For complicated structures, the resulting network may contain over several hundred thousand equivalent circuit components. Solving such a large circuit network is beyond the capability of existing circuit simulators. Method (c) can be obtained by applying various numerical methods such as the finite element method (FEM), the method of moments (MoM), etc. The dimension of the resultant matrix can exceed one million for surface discretization and 10 million for volume discretization. Thus, it is not practical to use such a large matrix to model the physical structure in circuit simulation.

For the above reasons, model order reduction (MOR) techniques [2]-[14] have been developed to approximate the original system by a simplified system with a much lower order. The lower-order system can be incorporated into circuit simulation for fast performance. The existing techniques in this area are reviewed in Chapter 2.

Traditional MOR methods require *a priori* knowledge of the original system; that is, the state-space expression of the original system is needed to generate the reduced-order system. However, in many practical problems, the only available information is the input-output characteristic of the system, where consequently the MOR cannot be applied. Hence, approaches based on curve-fitting techniques have been developed to generate

macromodels using rational functions directly from the input-output characteristic [15]-[22]. Since the systems of interest in this work are passive physical systems, the macromodels have to satisfy certain properties including real time domain response, causality, stability, and passivity. These requirements are discussed in detail in Chapter 3.

An efficient curve fitting technique using orthogonal polynomials is discussed in Chapter 4 to generate macromodels that satisfy physical constrains. The orthogonal polynomials are employed to avoid the ill-conditioned matrix resulted from the power series. Special treatments are conducted to guarantee the real time domain response and causality.

Passivity is an important issue in macromodeling. Interconnect and packaging structures are passive, so the constructed macromodel must be passive as well. Violation of passivity may cause unstable simulation results even connected to certain stable network [23]. Most of the existing methods enforce passivity after the macromodel is constructed [16], [24]-[26]. Chapter 5 describes various approaches of passivity enforcement techniques.

As the input data for the macromodeling process are obtained either from measurement or full-wave simulation, the data usually contain measurement or numerical noise and hence passivity might be violated. Although various approaches discussed in Chapter 5 can be used to generate passive macromodels, those approaches are valid under the condition that the passivity violation of the initial rational function obtained directly from curve fitting is relatively small. This is due to the perturbation nature of those passivity enforcement approaches. Our approach to avoid large passivity violation of the initial rational function is to perform passivity correction to the input data before the

curve fitting. Chapter 6 discusses the necessity and procedure to preprocess the input data including the noise filtering and passivity enforcement.

In Chapter 7, a new method is proposed to improve the modeling accuracy and efficiency, particularly for high-speed interconnects where the delay is an important physical characteristic. The new method is to model the black-box system as a cascade of a minimum phase subsystem, an all-pass subsystem, and a delay term. Thus, the time-domain delay can be explicitly extracted. On one hand, the time-domain delay itself is often a desirable parameter to be extracted in many practical applications. On the other hand, the system can be modeled more accurately with a lower order with the time delay extracted.

Chapter 8 concludes the work and proposes possible future work.

# 2 MODEL ORDER REDUCTION

## 2.1 Introduction

The increasing complexity involved in very large scale integration (VLSI) design demands efficient simulation techniques for larger and larger circuit systems. Particularly, to incorporate the electromagnetic effects in high-speed interconnect and packaging analysis, 3D distributed structures are modeled by Maxwell's equation or its approximate forms. These methods often result in a large matrix system. Due to the complexity of the 3D structures, the resultant matrix system often exceeds the capability of existing solvers if solved directly. In parallel, fast numeric algorithms that have been developed to accelerate the solution of large matrix systems, MOR methods are aimed at approximating the original high-order system with a lower-order system. Existing MOR methods include asymptotic waveform evaluation (AWE) method [2]-[4], Padé via Lanczos (PVL) method [5], block Arnoldi method [13], passive reduced-order interconnect macromodeling algorithm (PRIMA) [27], passive reduction algorithm with embedded state-space systems (PRESS) [28], etc.

The MOR methods have been applied to two types of problems: (a) large circuit network and the associated modified nodal analysis (MNA) matrix [29], [30], and (b) large discretized electromagnetic system and the associated matrix obtained from MoM, FEM, or PEEC method [1], etc. MOR methods generate a substitute system with a lower order than the original system. The reduced-order system is an approximation to the original one based on certain criteria.

Various MOR methods can all be cast into a general state-space expression [27] as follows:

$$\begin{cases} C\dot{x}_n = -Gx_n + Bu_N \\ i_N = L^T x_n \end{cases}$$

where the dimensions of the matrices are

$$C : M \times M,\ \ G : M \times M,\ B : M \times N,\ L : N \times M, \text{ and } N < M.$$

The transfer matrix $Y(s)$ satisfying $i_N(s) = Y(s)u(s)$ in the Laplace domain can be expressed as $Y(s) = L^T (G + sC)^{-1} B$. The goal of MOR methods is to approximate $Y(s)$ by $\hat{Y}(s) = \hat{L}^T (\hat{G} + s\hat{C})^{-1} \hat{B}$, where $\hat{G}$ and $\hat{C}$ are $P \times P$ matrices and $N \le P < M$. Various MOR methods differ from one another in three aspects: (a) means to construct the reduced order matrices, (b) criterion of approximation, and (c) means to preserve stability and passivity. That is, if the original system is stable and passive, the reduced order system should also be stable and passive.

## 2.2 Model Order Reduction Methods

MOR has been widely studied and applied to large-scale and distributed circuit analysis. The high-order system is represented by a lower-order system that can approximate the original system. The reduced-order system is then solved to get the system response.

### 2.2.1 Moment matching

Moment matching technique is applied in reducing the system order in the frequency domain. The AWE approach, which is a form of Padé approximation [6], is based on moment matching.

For moment matching, the solution to the MNA equation, as described in Equation (2.1):

$$Y(s)V(s) = J(s) \tag{2.1}$$

is expressed as

$$V(s) = Y^{-1}(s)J(s) = \sum_{i=0}^{\infty} M_i s^i \tag{2.2}$$

where $M_i$ is the *i*th moment of the system [29], [30]. The moments of the system can be calculated recursively [2]. The idea of the *P*th order moment matching is that the reduced order system is an approximation of the original system in the sense that they have the same first *P* moments. Padé approximation uses a rational function as in Equation (2.3) to approximate the first *P* moments as in the original system, where $P=M+N+1$:

$$\frac{b_0 + b_1 s + b_2 s^2 + \cdots + b_M s^M}{1 + a_1 s + a_2 s^2 + \cdots + a_N s^N} = M_0 + M_1 s + \cdots + M_{P-1} s^{P-1} \tag{2.3}$$

Although the Padé approximation has been intensively studied and widely applied [3], [7], [8], there are two major problems associated with it. One is its instability. The reduced-order poles obtained above are not necessarily in the left-half complex plane; thus, the resultant system could be unstable. Also, the passivity cannot be guaranteed. The other problem is that the ill-conditioned matrix associated with solving the reduced order poles when the order of the system is relatively high.

### 2.2.2 Krylov-subspace-based methods

In order to circumvent the ill-conditioning problem associated with moment matching, methods based on the Krylov subspace [9] have been developed. The idea is to approximate the original $M \times M$ matrix $A$ by a $P \times P$ matrix $\hat{A}$, where $P << M$ and $\hat{A}$

is the projection of $A$, on a Krylov subspace of dimension $P$. The Lanczos process [10] and block Arnoldi method [13] are two widely employed algorithms to generate the Krylov subspace.

In the *k*th iteration, Arnoldi algorithm generates an orthonormal basis $(v_0, v_1 \cdots v_{k-1})$ based on the Gram-Schmidt procedure with

$$span(V_k) = span(v_0, Av_0, \cdots A^{k-1}v_0) \tag{2.4}$$

Matrix $A$ is transformed into a lower-order upper Hessenberg matrix $H$ through $V$, resulting in

$$AV = VH$$

with $V^H V = I$, where the superscript $H$ is the complex conjugate transpose operator.

For Lanczos process, two orthogonormal basis vectors are formed based on $A$ and $A^H$, respectively. In the *k*th iteration, besides Equation (2.4), we also have

$$span(W_k) = span(w_0, A^H w_0, \cdots (A^H)^{k-1} w_0) \tag{2.5}$$

where $V$ and $W$ matrix are formed through three-term recurrence [11]. Original matrix $A$ is transformed into a reduced order tridiagonal matrix $T$ through

$$AV = W^H T,$$

with $W^H V = I$. The eigenvalues of the reduced order matrix $H$ or $T$ approximate those of the original matrix $T$.

The PVL [5] method and its extensions overcome the problem of solving the ill-conditioned matrix. However, the stability is still an issue, especially for the general $RLGC$ circuits.

### 2.2.3 Congruence transform

The congruence transform is applied with the PVL to guarantee the stability of the reduced order $RC$ circuits [12]. The transformation defines $B = V^H AV$ as the congruent of matrix $A$. The two matrices $B$ and $A$ have the same eigenvalues. Later, Arnoldi-based congruence transform is applied to guarantee the stability of $RLC$ circuits [13], [27].

In [31], integrated congruence transform is introduced to solve the distributed networks, characterized by the transmission line model as described in Equation (2.6).

$$\frac{\partial}{\partial z} v(z,t) = -Ri(z,t) - L\frac{\partial}{\partial t} i(z,t) \tag{2.6}$$

$$\frac{\partial}{\partial z} i(z,t) = -Gv(z,t) - C\frac{\partial}{\partial t} v(z,t)$$

where $R, L, G$, and $C$ are the resistance, inductance, conductance, and capacitance per unit length.

The Laplace transform of Equation (2.6) represents the system in frequency domain:

$$\frac{d}{dz} V(z,s) = -(R + sL) I(z,s) \tag{2.7}$$

$$\frac{d}{dz} I(z,s) = -(G + sC) V(z,s)$$

Assume $I(z,s) = u_i(z)\hat{x}(s)$ and $V(z,s) = u_v(z)\hat{x}(s)$, the integrated congruence transforms the $R$, $L$, $G$, and $C$ matrix to $\hat{R} = \int_0^1 u_i^T(z) R u_i(z) dz$, $\hat{L} = \int_0^1 u_i^T(z) L u_i(z) dz$, $\hat{G} = \int_0^1 u_v^T(z) G u_v(z) dz$ and $\hat{C} = \int_0^1 u_v^T(z) C u_c(z) dz$. The reduced-order model is solved

based on these congruent matrices. This algorithm solved the system with general *R, L, G, C* elements and guarantee the passivity preservation without first discretization of the transmission line.

## 2.3 Conclusion

Various MOR methods are reviewed and their advantages, disadvantages, and applicable conditions are discussed.

# 3 RATIONAL FUNCTION APPOXIMATION

## 3.1 Introduction

As the complexity of interconnects and packages keeps increasing and the clock speed gets faster and faster, the electromagnetic effects of distributed passive devices become an important issue in the system performance. These effects are usually captured either by full-wave electromagnetic simulation or by frequency-domain measurements in large amount of tabulated data. Therefore, the state-space model of the original system is not available. In other words, the internal mechanics of a complicated system may not have an explicit expression. While the MOR techniques described in Chapter 2 effectively solved the large-scale lumped and distributed circuits, it will not be applicable for the case when the only known information is the input-output characteristics of the system.

The time-domain response of such systems cannot be simulated directly by traditional circuit simulators such as SPICE [18]. And the MOR techniques discussed in the previous chapter are not capable of handling systems characterized by sampled data. A direct way to obtain the time-domain response is through inverse Fourier transform and direct convolution. However, the computational cost is too high due to the large number of frequency sampling points.

Polynomial is a straightforward approach for system approximation. However, it will be hard for polynomials to capture the characteristic of the system around its poles. There are other kinds of approximation methods, but all have certain limitations and are not suitable for black box modeling. Bode approximation is only good for real poles and

zeros [32], [33]. Padé approximation and its extensions use moments of the parameter around given frequency points and thus are dependent on the choice of the sampling frequency points [34], [35]. Digital filter design techniques solve similar problems but the frequency range is usually narrower and the problem size is smaller [36].

An efficient method to solve this problem is to use rational function as a black-box model to approximate the physical characteristics of a complicated system [11], [16], [18]. Rational functions will be able to capture the system characteristic around system poles. The internal details of the system are not required, and the system is modeled as a multiport network as shown in Figure 3.1.

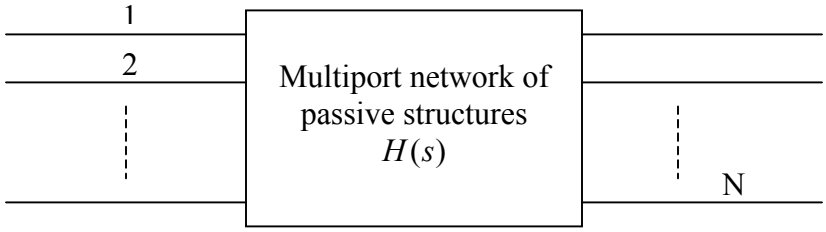


Figure 3.1 N-port black-box model.

$H(s)$ is the transfer function matrix of the system and can be expressed as in Equation (3.1):

$$H(s)=\begin{bmatrix} H_{11}(s) & \cdots & H_{1N}(s) \\ \vdots & H_{ij}(s) & \vdots \\ H_{N1}(s) & \cdots & H_{NN}(s) \end{bmatrix} \tag{3.1}$$

where $H_{ij}(s)$ is the input and output transfer function between ports $i$ and $j$. $H(s)$ can be either the scattering, admittance, or impedance matrices of the system.

The parameter matrix of the network, for instance, the $S$ parameter matrix, is approximated by rational functions of $s$, which is the complex frequency obtained from

Laplace transform. Each element of matrix $H(s)$ can be constructed by fitting the transfer function with the known sampled frequency-domain data.

The rational functions can be determined by various approaches from the input-output characteristic data of the multiport network. In this chapter, this widely used method is discussed as a context from which the work in this dissertation has been developed.

The systems of interest are passive physical structures. Therefore, more complicated than a mere curve-fitting problem, the constructed transfer functions (macromodels) must have real coefficients and must be causal, stable, and passive. In this chapter, we will first discuss the formulation of the macromodel. Then we will discuss the requirements of the macromodel and how to implement them. The process to ensure the first three features is discussed in this chapter; and the passivity enforcement will be discussed in Chapter 5. For clear illustration, we consider the one port case in the following discussion and it can easily be expanded to multiport cases.

## 3.2 Ordinary Power Series

High-speed interconnects or distributed circuits that are characterized by sampled frequency-domain data, can be represented by a rational function as described in Equation (3.2):

$$H(s) = \frac{b_0 + b_1 s + b_2 s^2 + \cdots + b_M s^M}{1 + a_1 s + a_2 s^2 + \cdots + a_N s^N} \tag{3.2}$$

where $a_0$ is normalized to 1.

The coefficients of $H(s)$ are determined by approximating the original system frequency response with the transfer function in (3.2) in the sense of lease square error [20]. Therefore, the problem is formulated as to determine all the coefficients, $M$, and $N$ in (3.2) to minimize (3.3).

$$\int_{S_i}^{S_f} \left| H(s) - H_{original}(s) \right|^2 ds \tag{3.3}$$

where $[S_i, S_f]$ is the interested frequency range.

In order to estimate the coefficients of the transfer function, Equation (3.2) is written in terms of the angular frequency $\omega$ as

$$H(j\omega) = \frac{b_0 + b_1(j\omega) + b_2(j\omega)^2 + \cdots + b_M(j\omega)^M}{1 + a_1(j\omega) + a_2(j\omega)^2 + \cdots + a_N(j\omega)^N} \tag{3.4}$$

Assume the total number of frequency samples is $K$, theoretically, the coefficients of the rational function can be obtained by solving Equation (3.5), which is the matrix form of Equation (3.4).

$$\begin{bmatrix} 1 & j\omega_0 & (j\omega_0)^2 & \cdots & (j\omega_0)^M & -j\omega_0 H(j\omega_0) & -(j\omega_0)^2 H(j\omega_0) & \cdots & -(j\omega_0)^N H(j\omega_0) \\ 1 & j\omega_1 & (j\omega_1)^2 & \cdots & (j\omega_1)^M & -j\omega_1 H(j\omega_1) & -(j\omega_1)^2 H(j\omega_1) & \cdots & -(j\omega_1)^N H(j\omega_1) \\ \vdots & \vdots & \vdots & & \vdots & \vdots & \vdots & & \vdots \\ 1 & j\omega_{K-1} & (j\omega_{K-1})^2 & \cdots & (j\omega_{K-1})^M & -j\omega_{K-1} H(j\omega_{K-1}) & -(j\omega_{K-1})^2 H(j\omega_{K-1}) & \cdots & -(j\omega_{K-1})^N H(j\omega_{K-1}) \end{bmatrix} \begin{bmatrix} b_0 \\ b_1 \\ b_2 \\ \vdots \\ b_M \\ a_1 \\ a_2 \\ \vdots \\ a_N \end{bmatrix} = \begin{bmatrix} H(j\omega_0) \\ H(j\omega_1) \\ \vdots \\ H(j\omega_{K-1}) \end{bmatrix} \tag{3.5}$$

Once the coefficients of $H(j\omega)$ are obtained by solving (3.5), the roots of the denominator will be obtained from

$$1 + a_1(j\omega) + a_2(j\omega)^2 + \cdots + a_N(j\omega)^N = 0 \tag{3.6}$$

Thus, the poles of the system will be available. Once we have the poles of the system, we can solve the residues of the system by writing the system transfer function in the partial fraction expansion as

$$H(j\omega) = k_0 + k_1(j\omega) + \sum_{i=1}^{N} \frac{r_i}{j\omega - p_i} \tag{3.7}$$

where $k_0$ and $k_1$ are the direct and proportional constants, which represents the conductance term and the shunt capacitance term [37]. Terms $p_i$ and $r_i$ are the *i*th poles and residues of the system, respectively. The transfer function will be obtained by solving the residues from Equation (3.7).

The above procedure will be straightforward if no constraints are imposed on the model. However, the macromodel is constructed to represent physically real systems, which are constrained to passive systems in this work. Therefore, besides solving the minimized least square error in Equation (3.3), the constructed model has to satisfy the following criteria so that a physically real system is guaranteed. (1) The coefficients are all real. In this case, the poles of the system are either real or in complex conjugate pairs. And the residues are correspondingly real or in complex conjugate pairs. (2) The system is causal and stable. Any physical system should be causal in the sense that the system should not have any response prior to the input. The system is stable so that the output is bounded under bounded input. This is guaranteed by enforcing the system poles on the left-half of the complex plane and the difference between the orders of the numerator and the denominator be less than or equal to one, that is, $|N - M| \le 1$ [16]. (3) The system is passive, which means the system does not generate any energy. Conditions (1) and (2) are necessary but not sufficient for passivity enforcement. We will discuss each requirements

of the model in detail below and find ways to guarantee the model to satisfy those requirements.

## 3.3 Stability

Stability is one characteristic that the macromodel needs to satisfy. A stable system means that the system has bounded output for all bounded input. The conditions for stability are $\int_{-\infty}^{\infty}|h(t)|dt<\infty$ for continuous systems and $\sum_{-\infty}^{\infty}|h(k)|<\infty$ for discrete systems [38].

In frequency domain, the transfer function needs to have all the poles in the left half of the complex plane. For each term $\frac{1}{s+a_i}$ corresponding to a real pole $-a_i$, the inverse Fourier transform gives the time domain response as $e^{-a_i t}$. For each complex conjugate pair poles $\frac{1}{s+\alpha_i+j\beta_i}+\frac{1}{s+\alpha_i-j\beta_i}$, the corresponding time domain response is $e^{-(\alpha_i+j\beta_i)t}+e^{-(\alpha_i-j\beta_i)t}=2\cos(\beta_i t)e^{-\alpha_i t}$. The overall time domain response is the sum of all terms:

$$\sum_i e^{-a_i t}+\sum_i 2\cos(\beta_i t)e^{-\alpha_i t} \tag{3.8}$$

In order for the system to have stable time domain response, each term in (3.8) has to converge as time goes to infinite. Therefore, all the real poles $-a_i$ and the real part of the complex poles $-\alpha_i$ should be negative. That is, all the poles of the macromodel should be in the left half of the complex plane.

## 3.4 Real Coefficients

### 3.4.1 The necessity for real coefficients

The macromodel of a physical system needs to have real coefficients. Otherwise, it will not provide real time domain response and hence cannot be physically implemented. The transfer function of the system $H(s)$, represented by the macromodel, is the Laplace transform of $h(t)$, where $H(s) = \int_{-\infty}^{\infty} h(t)e^{-st}dt$. For any physical system, the time domain response $h(t)$ is real during the whole time period. Therefore, the corresponding frequency domain response $H(s)$ is a rational function with real coefficients[18], [19].

The sufficient and necessary condition for the system transfer function to have real coefficients is that the poles of the system are either real or in complex conjugate pair. The residues for real poles need to be real, and the residues for complex conjugate pair poles need to be in complex conjugate pair. The direct and proportional term, they need to be real as well.

### 3.4.2 Guaranteeing real coefficients

Since complex frequency components are involved and the frequency response of the system is usually complex, it is hard to guarantee that the coefficients obtained by solving Equation (3.5) directly are real and that the resultant system is physical.

In order to obtain purely real coefficients, the real part of the frequency response is used in the approximation. The reasons to use the real part are: the real part of the frequency response is the even function of the original transfer function; the poles of the original function are the left half plane poles of those of the even function.

The real part of the system response can be expressed in the even function form as in Equation (3.9). The poles of the even function contain the poles of both $H(j\omega)$ and $H(-j\omega)$, with poles belonging to $H(j\omega)$ lie in the left half-plane:

$$\mathrm{Re}\{H(j\omega)\} = \frac{\hat{b}_0 + \hat{b}_1\omega^2 + \hat{b}_2\omega^4 + \cdots + \hat{b}_M\omega^{2M}}{1 + \hat{a}_1\omega^2 + \hat{a}_2\omega^4 + \cdots + \hat{a}_N\omega^{2N}} \tag{3.9}$$

In order to understand the relationship between poles of the original system and its real part, Forster's canonical model, which guarantees causality by the model itself, is used in showing the validity of the above statement. Equation (3.7) can be written as

$$H(j\omega) = k_0 + j\omega k_1 + \sum_{i=1}^{l} \frac{r_i}{j\omega - p_i} + \sum_{i=1}^{m} \left( \frac{x_i}{j\omega - q_i} + \frac{x_i^*}{j\omega - q_i^*} \right) \tag{3.10}$$

For clear illustration, we separate the real and imaginary poles here. Variable $p_i$ is the real pole of the system and lies in the left-half plane, and $r_i$ is the corresponding real residue. Variable $q_i$ is the complex pole and it appears in pair with its complex conjugate $q_i^*$, and the corresponding residues are also in complex conjugate pairs.

Let $q_i = u_i + jv_i$ and $x_i = a_i + jb_i$, where $u_i$, $v_i$, $a_i$, and $b_i$ are real and $u_i < 0$ for the sake of stability. The real part of the transfer function is

$$\mathrm{Re}\big(H(j\omega)\big) = k_0 + \mathrm{Re}\big(jk_1\omega\big) + \sum_{i=1}^{l} \mathrm{Re}\left( \frac{r_i}{j\omega - p_i} \right) + \sum_{i=1}^{m} \mathrm{Re}\left( \frac{a_i + jb_i}{j\omega - u_i - jv_i} + \frac{a_i - jb_i}{j\omega - u_i + jv_i} \right) \tag{3.11}$$

For the real pole, we have

$$\frac{r_i}{j\omega - p_i} = \frac{r_i(-p_i - j\omega)}{p_i^2 + \omega^2}$$

so the real part is $\frac{-r_i p_i}{p_i^2 + \omega^2}$. The corresponding poles of the real part are $\pm jp_i$ in terms of $\omega$.

For the complex conjugate pair poles,

$$\mathrm{Re}\left( \frac{a_i + jb_i}{j\omega - u_i - jv_i} + \frac{a_i - jb_i}{j\omega - u_i + jv_i} \right) = \frac{-a_i u_i - b_i(\omega - v_i)}{u_i^2 + (\omega - v_i)^2} + \frac{-a_i u_i - b_i(\omega + v_i)}{u_i^2 + (\omega + v_i)^2}$$

the poles of the real part are $\pm v_i \pm ju_i$ in terms of $\omega$.

From the above observation, it is obvious that the poles of the real part of any transfer function are closely related to those of the transfer function itself. In the above discussion, poles of the real part are expressed in terms of the angular frequency $\omega$ and poles of the original function are in terms of the complex frequency $s$. Therefore, there is a factor of imaginary unit $j$.

The poles of the even function are multiplied by $j$ to transform the poles from $s$ domain to $\omega$ domain. In order for the original system to be asymptotic stable, only those poles that lie in the left half plane are the poles of the original system.

Figure 3.2 shows the relationship between the poles of a system and those of its corresponding real part.

From Figure 3.2, it is obvious that the poles of an even function are symmetric about the imaginary axis. The poles for the original stable system are the poles that are in the left half of the complex plane, as shown by the diamond points in the figure.

### 3.4.3 Approximation with real coefficients guaranteed

As discussed previously, the poles of the original system can be obtained from the poles of the real part of the frequency response. Therefore, the coefficients/poles of the

original system can be obtained by fitting the real part of the frequency response with the even rational polynomial function of the squared variable as shown in Equation (3.9).

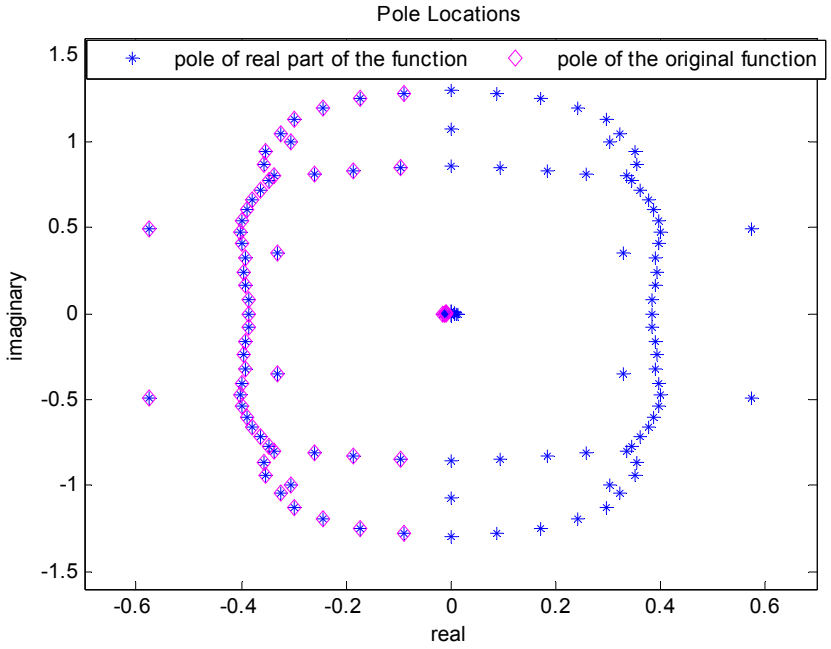


Figure 3.2 Comparison of poles of a system with poles of its real part.

The matrix associated with solving the denominator coefficients is a Vandermonde-like matrix as shown in Equation (3.12):

$$\begin{bmatrix} 1 & \omega_0^2 & \omega_0^4 & \cdots & \omega_0^{2M} & -\omega_0^2\,\mathrm{Re}(H(j\omega_0)) & -\omega_0^4\,\mathrm{Re}(H(j\omega_0)) & \cdots & -\omega_0^{2N}\,\mathrm{Re}(H(j\omega_0)) \\ 1 & \omega_1^2 & \omega_1^4 & \cdots & \omega_1^{2M} & -\omega_1^2\,\mathrm{Re}(H(j\omega_1)) & -\omega_1^4\,\mathrm{Re}(H(j\omega_1)) & \cdots & -\omega_1^{2N}\,\mathrm{Re}(H(j\omega_1)) \\ \vdots & \vdots & \vdots & & \vdots & \vdots & \vdots & & \vdots \\ 1 & \omega_{K-1}^2 & \omega_{K-1}^4 & \cdots & \omega_{K-1}^{2M} & -\omega_{K-1}^2\,\mathrm{Re}(H(j\omega_{K-1})) & -\omega_{K-1}^4\,\mathrm{Re}(H(j\omega_{K-1})) & \cdots & -\omega_{K-1}^{2N}\,\mathrm{Re}(H(j\omega_{K-1})) \end{bmatrix} \begin{bmatrix} \hat{b}_0 \\ \hat{b}_1 \\ \hat{b}_2 \\ \vdots \\ \hat{b}_M \\ \hat{a}_1 \\ \hat{a}_2 \\ \vdots \\ \hat{a}_N \end{bmatrix} = \begin{bmatrix} \mathrm{Re}(H(j\omega_0)) \\ \mathrm{Re}(H(j\omega_1)) \\ \vdots \\ \mathrm{Re}(H(j\omega_{K-1})) \end{bmatrix}$$

(3.12)

Once the coefficients are obtained by solving (3.12), the roots of the even function will be obtained from

$$1+\hat{a}_1\omega^2+\hat{a}_2\omega^4+\cdots+\hat{a}_N\omega^{2N}=0 \tag{3.13}$$

which gives the poles of the even function. By multiplying the poles with $j$ and taking only the stable poles in the left half-plane, the poles of the original transfer function can be obtained.

However, Equation (3.12) becomes ill-conditioned or even singular for a wide frequency range and high-order approximation since the entries of the matrix is the power series [11]. This is because the ordinary power series $\{\omega^0,\omega^1,\omega^2,\omega^3,\cdots\}$ have a very large dynamic range [22]. We will solve this problem in Chapter 4.

## 3.5 Causality

Any real system is causal. In time domain, causality means that the system output at time $t=t_0$ depends only on the inputs at $t\le t_0$. The causality criterion requires that the system impulse response $h(t)$ is null for time $t<0$ [38].

Since the system responses in frequency and time domain are related by the Laplace transform, the macromodel $H(s)$, which approximate the real system in the frequency domain, is also subject to the causality requirement. The Laplace transform $H(s)=\int_{-\infty}^{\infty}h(t)e^{-st}dt$ becomes $H(s)=\int_{0}^{\infty}h(t)e^{-st}dt$ since $h(t)=0$ for $t<0$. As a result of the causality, the real and imaginary part of the frequency domain response satisfy the Hilbert transform [38].

To illustrate the relationship between the real and imaginary part of the frequency response of a causal system, we write the time domain system response in terms of its even and odd components. Since the frequency response is in the form of sampling points, the discrete case will be studied.

Any time domain sequence $h(n)$ can be expressed as $h(n) = h_e(n) + h_o(n)$, where $h_e(n) = \frac{1}{2}[h(n) + h(-n)]$ and $h_o(n) = \frac{1}{2}[h(n) - h(-n)]$ are the even and odd components of $h(n)$. And

$$h(n) = 2h_e(n)u(n) - h_e(0)\delta(n)$$

$$h(n) = 2h_o(n)u(n) + h(0)\delta(n)$$

where $u(n)$ and $\delta(n)$ are the unit step and unit sample sequence. For the stable system, its Fourier transform exists and is defined as

$$H(j\omega) = H_R(j\omega) + jH_I(j\omega),$$

where $H(j\omega)$ is the system response in the frequency domain, $H_R(j\omega)$ and $H_I(j\omega)$ are the corresponding real and imaginary parts of the frequency response. When the system response is real, $H_R(j\omega)$ is the Fourier transform of $h_e(n)$ and $H_I(j\omega)$ is the Fourier transform of $h_o(n)$ [38].

For causal systems, $h(-n)$ is zero, and the system $h(n)$ can be completely determined by $h_e(n)$. Similarly, $H_R(j\omega)$ will determine the frequency response $H(j\omega)$. And obviously, the imaginary part of the frequency response $H_I(j\omega)$ can be obtained from $H_R(j\omega)$ as well. From [38], $H_R(j\omega)$ and $H_I(j\omega)$ are related by the Hilbert transform as described in

$$H_R(j\omega) = h(0) + \frac{1}{2\pi} P\int_{-\pi}^{\pi} H_I(j\theta)\cot(\frac{\omega-\theta}{2})d\theta$$

$$H_I(j\omega) = -\frac{1}{2\pi} P\int_{-\pi}^{\pi} H_R(j\theta)\cot(\frac{\omega-\theta}{2})d\theta$$

where *P* denotes the Cauchy principal value of the following integrals.

When dealing with the discrete data, the discrete Hilbert transform is applied,

$$H_I(j\omega)_k = \begin{cases} -\frac{2}{\pi}\sum_{n\ odd}\frac{H_R(j\omega)_n}{k-n} \\ -\frac{2}{\pi}\sum_{n\ even}\frac{H_R(j\omega)_n}{k-n} \end{cases}$$

where $H_I(j\omega)_k$ and $H_R(j\omega)_n$ are the *k*th and *n*th samples of the corresponding frequency response.

In order to guarantee causality of the system, the frequency domain data need to be modified if there are causality violations. That is, to ensure the real and imaginary parts of the data to satisfy the Hilbert transform as described in the above equations.

Below is an example showing the causality violation and restoration of the measured data from transmission lines. Figure 3.3(a) shows the imaginary part of the data from measurement and from calculation based on the Hilbert transform. Figure 3.3(b) shows the measured and calculated magnitude. In both figures, the solid and the dashed curve have the same corresponding real part. The solid curve shows the original measured data, while the dashed curve shows the calculated data from the Hilbert transform.

From the above discussion, the imaginary part can be obtained from the real part for causal systems. We can have both the magnitude and phase information from the real part of the frequency response only. Therefore, only the real part of the frequency response will be used in finding the poles of the system and the causality will be automatically satisfied. This way of dealing the data is also consistent with the requirements in guaranteeing the real coefficients. Similarly, the real part of the frequency response is used to find residues and keep the causality. In this work, both the

real and imaginary components of the frequency response are used in approximating the residues. In order to guarantee the time domain response of the system is causal (zero for time less than zero), the data represented by the dashed curve should be used when the imaginary information is needed.

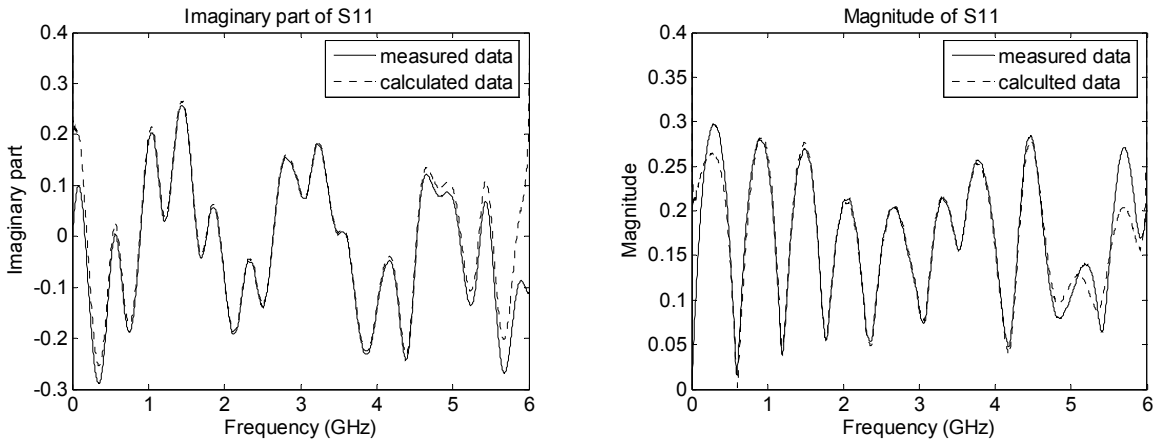


Figure 3.3 (a) Comparison of the imaginary part of the measured and calculated data. (b) Comparison of the magnitude of the measured and calculated data.

## 3.6 Passivity

The macromodel for any passive system should be passive as well. A passive system means that the system will only absorb but not generate any energy [39]. Mathematically, it means that the system transfer matrix is positive real for the admittance ($Y$), impedance ($Z$), transmission ($T$), or the hybrid ($H$) matrix and bounded real for the scattering matrix [39].

Violation of passivity will lead to unstable transient response when the system is connected to the rest of the circuits [23], [40]. If the macromodel is stable but not passive, unstable poles may occur when the system characterized by the macromodel is connected with other part of the circuits. However, a stable and passive macromodel will guarantee stability of the whole system it is in.

Assume $H(s)$ is the transfer matrix of a multiport system and represents the *Y, Z*, *T*, or *H* matrix. The system is passive [23], [41], if

1. $H(s^*) = H^*(s)$, where '$^*$' is the complex conjugate operator;
2. $H(s)$ is positive real. For any vector $z$, $z^*[H^T(s^*) + H(s)]z \geq 0$ for all values of $s$ with $\mathrm{Re}(s) > 0$.

If $H(s)$ represents the scattering parameter matrix *S*, the system is passive [43], if

1. $H(s^*) = H^*(s)$;
2. $H(s)$ is bounded real. For any $s = j\omega$,

$$I - H^T(j\omega^*)H(j\omega) \geq 0$$

which means that $\max(\sigma(H(j\omega))) \leq 1$ for any $\omega$, where $\sigma(H(j\omega)$ is the singular value of $H(j\omega)$.

The requirements for real coefficients, causality and stability are usually enforced as the model is constructed. Passivity, however, can be enforced either when the model is built or afterwards. Detailed discussion on passivity enforcement will be found in Chapter 5.

## 3.7 Conclusion

Several requirements for the macromodel are discussed based on the properties of the physical system. Real coefficients, causality, stability and passivity are all need to be satisfied by the macromodel. For each requirement, method has been proposed to guarantee that the macromodel satisfy the criterion and thus can be implemented in real system.

# 4 ORTHOGONAL POLYNOMIAL APPROACH

## 4.1 Introduction

In Chapter 3, the macromodel is discussed to represent systems characterized by frequency domain data. The macromodel takes the form of the rational function and satisfies the requirements of having real coefficients, causal, stable and passive. Instead of working on the rational function directly, the even function, which corresponds to the real part of the frequency response is applied. By doing this, we can guarantee that the first three requirements of the macromodel are met. The validation and implementation of the methods are discussed in Chapter 3.

However, direct formulation by ordinary power series will result in an ill-conditioned matrix equation. Both Equations (3.5) and (3.12) are the Vandermonde-like matrices, which become ill-conditioned or even singular for wide frequency range or high-order approximation.

Different methods have been proposed to overcome this problem. Frequency shift and normalization has been proposed in [18]. By the shift and normalization, frequency range is mapped from $[\omega_{\min}, \omega_{\max}]$ to $[-1,1]$ and leads to a much better matrix condition number. Although there are improvements by using the frequency normaliztion, it still cannot completely solve the problem when the frequency range is wide and the problem size is huge.

Partition over the frequency helps improve the matrix condition number by reducing the problem size [8], [44], [45]. The method approximates the system in different

frequency bands separately and repeats the process recursively until all frequencies are well approximated. Since the approximation in each frequency band does not consider the influence of the approximation from other bands, the method may converge very slow and thus not efficient.

There are also methods like Householder orthogonal triangularization [11] and singular value decomposition [46] that solve matrix equation more efficiently. However, if the singular values of a matrix are not reasonably spread, which always occurs for large problem size with a wide frequency range, accurate solution will not be obtained.

Chebyshev of the first kind, a special case of the orthogonal polynomials, is employed [15]-[17], [22] to solve the ill-conditioned problem. Since it changes the matrix itself, accurate approximation can be obtained.

In this chapter, we will investigate and implement the general orthogonal polynomials on the black-box modeling. The properties of the orthogonal polynomials will be discussed. Clenshaw's recurrence algorithm is used to transform the coefficients of the orthogonal polynomials to those of the ordinary power series. The model order estimation and effects of the sampling points are discussed as well.

## 4.2 Orthogonal Polynomials

To overcome the aforementioned problem, orthogonal polynomials are used in the approximation. Classical orthogonal polynomials defined over interval [-1,1] are considered in this work. The Legendre and Cheybshev of the first and second kind polynomials are suitable for this problem because they have remarkable properties in the

interval [-1,1]. These are special cases of the more general Jacobi or Gegenbauer polynomials. Jacobi polynomials are defined as

$$P_n^{(\alpha,\beta)}(x) = 2^{-n}\sum_{k=0}^{n}\binom{n+\alpha}{k}\binom{n+\beta}{n-k}(x-1)^{n-k}(x+1)^k \tag{4.1}$$

The Jacobi polynomials $P_n^{(\alpha,\beta)}(x)$ are generated by applying the orthogonalization step of the Gram-Schmidt process to the standard basis $\{1,x,x^2,x^3,\cdots\}$ of $P$[-1,1] with respect to the weight function given by the following continuous beta distribution on the interval [-1,1]:

$$w^{(\alpha,\beta)}(x) = (1-x)^{\alpha}(1+x)^{\beta}, \text{ for } \alpha > -1, \beta > -1 \tag{4.2}$$

The Jacobi polynomials reduce to Gegenbauer polynomials, $C_n^{\lambda}(x)$ when $\alpha = \beta = \lambda - \frac{1}{2}$, in (4.1) and (4.2). The Jacobi also reduces to Chebyshev of the first and second kinds as well as Lengendre series when the parameters α and β are set to $-\frac{1}{2}$, $\frac{1}{2}$, and 0, respectively. The hierarchy of the common special orthogonal polynomials over a compact interval, $[\omega_{min}, \omega_{max}]$, are summarized in Figure 4.1.

For simplicity, we transform the interval $[\omega_{min}, \omega_{max}]$ into the interval [-1,1] using the one-to-one continuous mapping given by

$$\varpi = \left(\frac{\omega - \omega_{min}}{\omega_{max} - \omega_{min}}\right) - 1 \tag{4.3}$$

where $\omega_{min}$, and $\omega_{max}$ are the lowest and highest frequencies, respectively, and thus $\varpi$ is the normalized frequency.

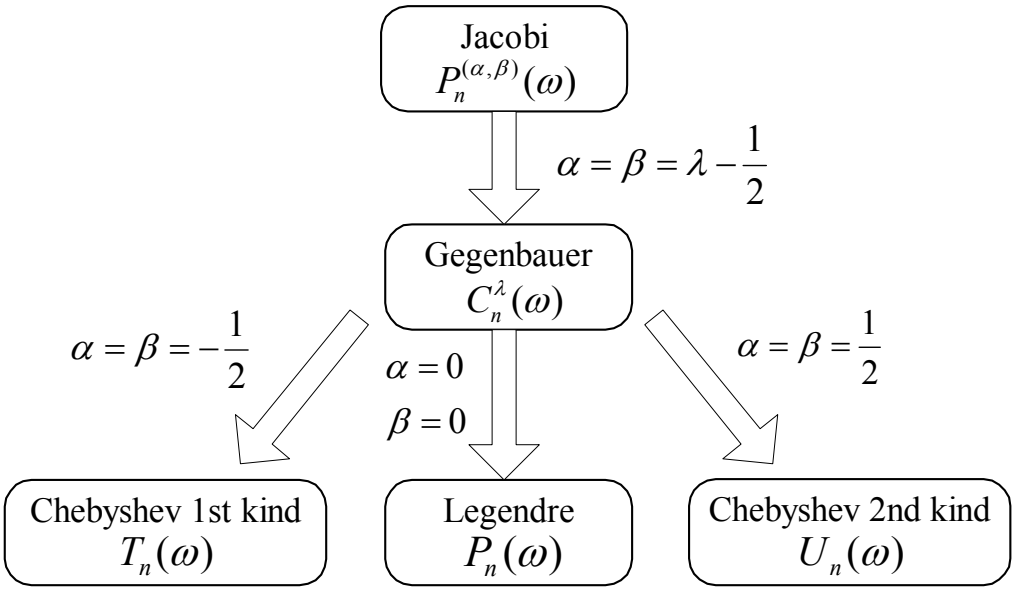


Figure 4.1 Hierarchy of common orthogonal polynomials of the finite interval.

Some of the important properties of the special orthogonal functions are shown in Table 4.1. These properties include the following:

- Simple generating expressions
- Polynomial nature and orthogonality with respect to the weight functions
- Three-term recurrence relations

Table 4.1: Special orthogonal polynomials

| **Function** | **Expression** | **Weight** | **Recurrence Relation** |
|---|---|---|---|
| *Chebyshev First Kind* | $T_n(x) = \cos(n\cos^{-1}x)$ | $(1-x^2)^{-1/2}$ | $T_{n+1}(x) = 2xT_n(x) - T_{n-1}(x)$<br>$T_0(x) = 1, \quad T_1(x) = x$ |
| *Chebyshev Second Kind* | $U_n(x) = \frac{\sin((n+1)\cos^{-1}x)}{\sin(\cos^{-1}x)}$ | $(1-x^2)^{1/2}$ | $U_{n+1}(x) = 2xU_n(x) - U_{n-1}(x)$<br>$U_0(x) = 1, \quad U_1(x) = 2x$ |
| *Legendre* | $L_n(x) = 2^{-n}\sum_{k=0}^{n/2}(-1)^k\binom{n}{k}\binom{2n-2k}{n}x^{n-2k}$ | 1 | $(n+1)L_{n+1}(x) = (2n+1)xL_n(x) - nL_{n-1}(x)$<br>$L_0(x) = 1, \quad L_1(x) = x$ |

For higher order terms, the power series become very similar or parallel over most of the interval as shown in Figure 4.2(a). On the other hand, the terms of Legendre, Chebyshev of the first and second kinds show quite different shapes and are not parallel over the entire intervals. They also have a small dynamic range of the entire interval as shown in Figure 4.2(b), (c), and (d). Therefore, the orthogonal polynomials are well suited for higher-order interpolation problems [47].

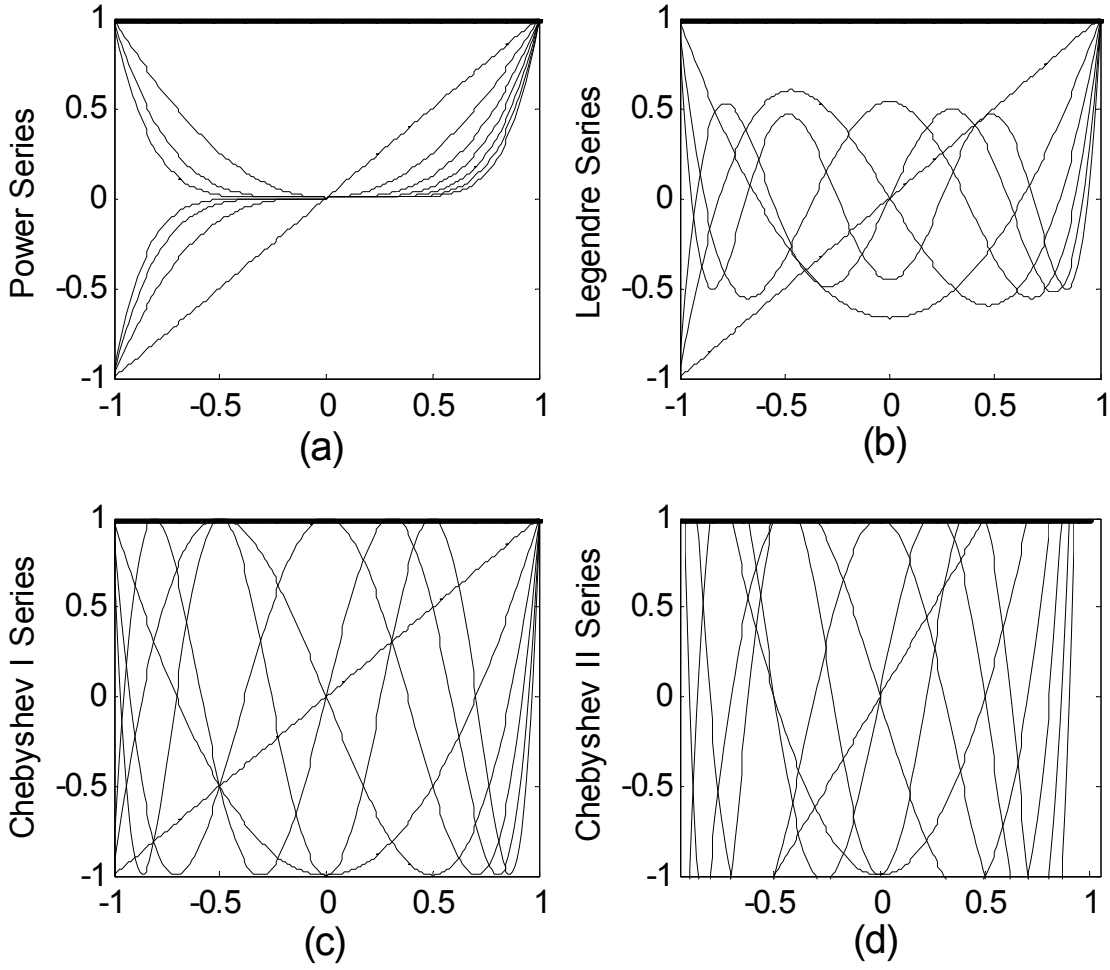


Figure 4.2 Power series and three special orthogonal polynomials. (a) Power series, (b) Legendre series, (c) Chebyshev of the first kind, and (d) Chebyshev of the second kind.

To apply the orthogonal polynomials, the frequency must be normalized to the desired range by performing a change of variables using (4.3). Instead of the power

series, the system transfer function described in (3.4) can be written using one of the orthogonal polynomials, $F_k(x)$, of Table 4.1.

$$H(j\varpi) = \frac{b_0' F_0(j\varpi) + b_1' F_1(j\varpi) + b_2' F_2(j\varpi)^2 + \cdots + b_M' F_M(j\varpi)^M}{1 + a_1' F_1(j\varpi) + a_2' F_2(j\varpi)^2 + \cdots + a_N' F_N(j\varpi)^N}$$

The corresponding even function associated with the real part of the system response is

$$\mathrm{Re}\big(H(j\varpi)\big) = \frac{\tilde{b}_0 F_0(j\varpi) + \tilde{b}_1 F_2(j\varpi) + \tilde{b}_2 F_4(j\varpi) + \cdots + \tilde{b}_M F_{2M}(j\varpi)}{1 + \tilde{a}_1 F_2(j\varpi) + \tilde{a}_2 F_4(j\varpi) + \cdots + \tilde{a}_N F_{2N}(j\varpi)}$$

When the orthogonal polynomials are used, the interpolation matrix of (3.12) is modified into (4.4). Once the coefficients $\tilde{a}'s$ and $\tilde{b}'s$ of the orthogonal polynomials are found, Clenshaw's recurrence algorithm is used to efficiently and accurately calculate the coefficients of the corresponding power series.

$$Ax = b \tag{4.4}$$

where

$$A = \begin{bmatrix} 1 & F_2(\tilde{\omega}_0) & \cdots & F_{2M}(\tilde{\omega}_0) & -F_2(\tilde{\omega}_0)\mathrm{Re}(H(j\omega_0)) & \cdots & -F_{2N}(\tilde{\omega}_0)\mathrm{Re}(H(j\omega_0)) \\ 1 & F_2(\tilde{\omega}_1) & \cdots & F_{2M}(\tilde{\omega}_1) & -F_2(\tilde{\omega}_1)\mathrm{Re}(H(j\omega_1)) & \cdots & -F_{2N}(\tilde{\omega}_1)\mathrm{Re}(H(j\omega_1)) \\ & & & \vdots & \vdots & & \\ 1 & F_2(\tilde{\omega}_{K-1}) & \cdots & F_{2M}(\tilde{\omega}_{K-1}) & -F_2(\tilde{\omega}_{K-1})\mathrm{Re}(H(j\omega_{K-1})) & \cdots & -F_{2N}(\tilde{\omega}_{K-1})\mathrm{Re}(H(j\omega_{K-1})) \end{bmatrix}$$

$$x^T = \begin{bmatrix} \tilde{b}_0 & \tilde{b}_1 & \tilde{b}_2 & \cdots & \tilde{b}_M & \tilde{a}_1 & \tilde{a}_2 & \cdots & \tilde{a}_N \end{bmatrix}$$

$$b^T = \begin{bmatrix} Re\big(H(j\omega_0)\big) & Re\big(H(j\omega_1)\big) & \cdots & Re\big(H(j\omega_{K-1})\big) \end{bmatrix}$$

## 4.3 Clenshaw's Recurrence Formula

In [18], [48], Clenshaw's formula is given for the general function that has a three-term recursive relationship of the form

$$F_{n+1}(x) = \alpha(n,x)F_n(x) + \beta(n-1,x)F_{n-1}(x) \tag{4.5}$$

where $\alpha(n,x)$ and $\beta(n,x)$ are functions in the recurrence relation. For Chebyshev polynomials, $\alpha(n,x)$ is $2x$ and $\beta(n,x)$ is $-1$. For Legendre polynomials, $\alpha(n,x)$ is $\frac{2n+1}{n+1}$ and $\beta(n,x)$ is $\frac{-n}{n+1}$.

For a 2*N*th order system, it can be described as

$$f(\varpi) = \sum_{i=0}^{2N} \tilde{a}_i F_i(\varpi) = \sum_{i=0}^{2N} \hat{a}_i \varpi^i \tag{4.6}$$

The transformation between the $\tilde{a}$'s and $\hat{a}$'s can be made by applying the following recurrence formulas.

Defining $y_{2N+2} = y_{2N+1} = 0$ and $y_k = \alpha(k,\varpi)y_{k+1} + \beta(k,\varpi)y_{k+2} + \tilde{a}_k$, we will have

$$\begin{aligned} y_{2N} &= \tilde{a}_{2N} \\ y_{2N-1} &= \alpha(2N-1,\varpi)y_{2N} + \tilde{a}_{2N-1} \\ &\vdots \\ y_2 &= \alpha(2,\varpi)y_3 + \beta(2,\varpi)y_4 + \tilde{a}_2 \end{aligned} \tag{4.7}$$

Solving the above equations for $\tilde{a}$'s on the right-hand side, Equation (4.6) becomes

$$\begin{aligned} f(\varpi) = {} & +\cdots+[y_7 - \alpha(7,\varpi)y_8 - \beta(7,\varpi)y_9]F_7(\varpi) + [y_6 - \alpha(6,\varpi)y_7 - \beta(6,\varpi)y_8]F_6(\varpi) + [y_5 - \alpha(5,\varpi)y_6 - \beta(5,\varpi)y_7]F_5(\varpi) \\ & +\cdots+[y_2 - \alpha(2,\varpi)y_3 - \beta(2,\varpi)y_4]F_2(\varpi) + [y_1 - \alpha(1,\varpi)y_2 - \beta(1,\varpi)y_3]F_1(\varpi) + [\tilde{a}_0 - \beta(0,\varpi)y_2 + \beta(0,\varpi)y_2]F_0(\varpi) \end{aligned}$$

(4.8)

Examining the terms containing $y_7$ shows that

$$y_7[F_7(\varpi)-\alpha(6,\varpi)F_6(\varpi)-\beta(5,\varpi)F_5(\varpi)]=0$$

as a consequence of the recurrence relation. Similar expressions can be obtained for other $y_k$'s down through $y_2$. The only remaining terms in (4.8) are

$$f(\varpi)=\beta(0,\varpi)y_2F_0(\varpi)+\tilde{a}_0F_0(\varpi)+F_1(\varpi)y_1$$

where $y_1$ and $y_2$ can be obtained from (4.7). Then $f(\varpi)$ can be converted into a power series, which is an even function in terms of $\varpi^2$.

Following the conversion of the coefficients of the orthogonal polynomials to the coefficients of the ordinary power series, poles of the system can be obtained by finding the roots of the denominator polynomials.

After the poles of the system are found, the residues can be obtained through the partial fraction expansion of the transfer function. In order to make sure that the residues are in complex conjugate pairs, we must rewrite the system transfer function in the manner described in [47] as

$$H(j\omega)=k_0+k_1(j\omega)+\frac{r_1}{j\omega-p_1}+\frac{r_1^*}{j\omega-p_1^*}+\cdots\frac{r_m}{j\omega-p_m}+\frac{r_m^*}{j\omega-p_m^*}+\frac{r_{m+1}}{j\omega-p_{m+1}}+\cdots+\frac{r_{m+n}}{j\omega-p_{m+n}} \quad (4.9)$$

This can be written as

$$H(j\omega)=k_0+k_1(j\omega)+\frac{r_{1r}+jr_{1i}}{j\omega-p_1}+\frac{r_{1r}-jr_{1i}}{j\omega-p_1^*}+\cdots+\frac{r_{mr}+jr_{mi}}{j\omega-p_m}+\frac{r_{mr}-jr_{mi}}{j\omega-p_m^*}+\frac{r_{m+1}}{j\omega-p_{m+1}}+\cdots+\frac{r_{m+n}}{j\omega-p_{m+n}} \quad (4.10)$$

By doing this, it is guaranteed that the two residues of a pair of complex conjugate poles are in a complex conjugate pair as well.

The matrix equation for solving the real and imaginary parts of the residues is

$$\tilde{A}\tilde{x} = \tilde{b} \tag{4.11}$$

where $\tilde{A}$ is expressed as

$$\tilde{A}=\begin{bmatrix} 1 & j\omega_0 & \frac{1}{j\omega_0-p_1}+\frac{1}{j\omega_0-p_1^*} & \frac{j}{j\omega_0-p_1}-\frac{j}{j\omega_0-p_1^*} & \cdots & \frac{1}{j\omega_0-p_m}+\frac{1}{j\omega_0-p_m^*} & \frac{j}{j\omega_0-p_m}-\frac{j}{j\omega_0-p_m^*} & \frac{1}{j\omega_0-p_{m+1}} & \cdots & \frac{1}{j\omega_0-p_{m+n}} \\ 1 & j\omega_1 & \frac{1}{j\omega_1-p_1}+\frac{1}{j\omega_1-p_1^*} & \frac{j}{j\omega_1-p_1}-\frac{j}{j\omega_1-p_1^*} & \cdots & \frac{1}{j\omega_1-p_m}+\frac{1}{j\omega_1-p_m^*} & \frac{j}{j\omega_1-p_m}-\frac{j}{j\omega_1-p_m^*} & \frac{1}{j\omega_1-p_{m+1}} & \cdots & \frac{1}{j\omega_1-p_{m+n}} \\ \vdots & & \vdots & \vdots & & \vdots & \vdots & & & \vdots \\ 1 & j\omega_{k-1} & \frac{1}{j\omega_{k-1}-p_1}+\frac{1}{j\omega_{k-1}-p_1^*} & \frac{j}{j\omega_{k-1}-p_1}-\frac{j}{j\omega_{k-1}-p_1^*} & \cdots & \frac{1}{j\omega_{k-1}-p_m}+\frac{1}{j\omega_{k-1}-p_m^*} & \frac{j}{j\omega_{k-1}-p_m}-\frac{j}{j\omega_{k-1}-p_m^*} & \frac{1}{j\omega_{k-1}-p_{m+1}} & \cdots & \frac{1}{j\omega_{k-1}-p_{m+n}} \end{bmatrix}$$

and

$$\tilde{x}^T = \begin{bmatrix} k_0 & k_1 & r_{1r} & r_{1i} & \cdots & r_{mr} & r_{mi} & r_{m+1} & \cdots & r_{m+n} \end{bmatrix},$$

$$\tilde{b}^T = \begin{bmatrix} H(j\omega_0) & H(j\omega_1) & \cdots & H(j\omega_k) \end{bmatrix}$$

To guarantee that all the $\tilde{x}$'s are real, Equation (4.11) can be written as

$$\begin{bmatrix} \tilde{A}' \\ \tilde{A}'' \end{bmatrix} \tilde{x} = \begin{bmatrix} \tilde{b}' \\ \tilde{b}'' \end{bmatrix}, \tag{4.12}$$

where $\tilde{A}'$ and $\tilde{A}''$ are the real and imaginary parts of matrix $\tilde{A}$, and $\tilde{b}'$ and $\tilde{b}''$ are the real and imaginary parts of vector $\tilde{b}$. Equation (4.12) solves the direct and proportional term, the real residues, and the real and imaginary part of the complex residues.

The algorithm of rational function approximation through orthogonal polynomials and the Clenshaw's recurrence formula is given in pseudocode in Algorithm 4.1.

**Algorithm 4.1:** Rational function approximation

1. *Read in the frequency domain data. Transform the data into real and imaginary format if necessary.*

2. *Normalize and shift the frequency: map* $[\omega_{\min}, \omega_{\max}]$ *into* $[-1,1]$ *using Equation (4.3).*
3. *Construct the real matrix Equation (4.4), with the real part of the frequency response.*

$$A \in R^{K\times(M+N+1)},\ x \in R^{M+N+1},\ b \in R^{K}$$

4. *Solve Equation (4.4) for the coefficient vector* $x$*. The least square solution is obtained.*
5. *Transfer the coefficients of the orthogonal polynomials to coefficients of the power series for the normalized frequency.*
6. *Find the coefficients in terms of the unnormalized frequency.*
7. *Solve the roots of the even function from coefficients obtained in step 6). The left half plane poles are poles for the original system.*
8. *Solve residues of the system by Equation (4.12).*

## 4.4 Order Estimation

In the algorithm developed above, it is assumed that the order of the system is known, that is, $M$ and $N$ are known. However, it is not a trivial problem to determine the appropriate order from the simulated or measured data. When an inappropriate order is used, there is no way to reduce the large error between the original and the approximated systems.

There are several ways to estimate the order of the LTI (linear time invariant) system, such as Akaike information criterion (AIC) [49], minimum description length (MDL) [50], and minimum description complexity (MDC) [51]. However, these methods are all valid in the time domain and are not suitable for frequency domain analysis. In [52], the order is estimated by the minimum eigenvalue tracking method, where the minimum eigenvalue of the matrix associated with solving the coefficients is plotted as a function of the system order, as shown in Figure 4.3 [16]. The optimum order is found when the eigenvalue stops its steepest decrease. The singular value decomposition (SVD) method is applied in [46] to estimate the order of the rational

function. The total least square (TLS) is used to solve for the coefficients and finds the nonzero eigenvalues.

The above two methods work well for low order systems. However, when the system order becomes high, the Vandermonde-like matrix in Equation (3.5) for finding the eigenvalues becomes ill-conditioned and the effectiveness of the method is greatly impaired.

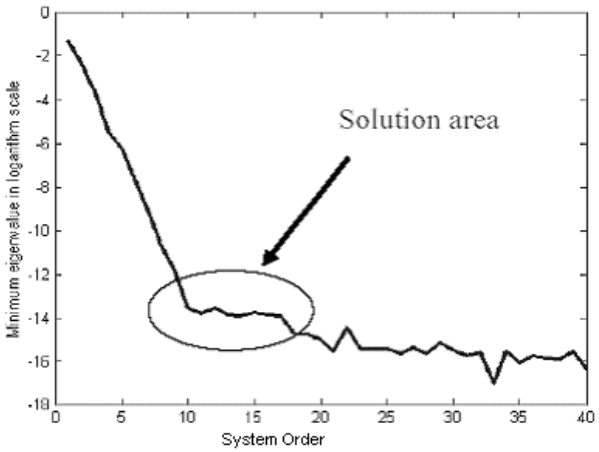


Figure 4.3 Minimum eigenvalue vs. system order.

However, orthogonal polynomials can be applied here to alleviate the problem. From the recurrence relation described in Table 4.1, it is shown that the Nth order of the orthogonal polynomials has the same order as the power series. Therefore, functions described in Equation (4.6) have the same order for ordinary power series and the orthogonal polynomials. And we can find the order of the system through the orthogonal system.

The number of data points needed will be discussed more in later. For now, we assume that we have enough data points $K$, which means $K \gg M+N+1$. Matrix $A$ in Equation (4.4) is an overdetermined system, and the least square solution is used. By

minimizing $\|Ax-b\|_2$, where $A \in \mathbb{R}^{K\times(M+N+1)}$ and $b \in \mathbb{R}^K$, the solution of $x \in \mathbb{R}^{M+N+1}$ will be $X = \left\{ x \in \mathbb{R}^{M+N+1} \middle| \|Ax-b\|_2 = \min \right\}$ and has the following properties [16], [53]:

- $x \in X \Leftrightarrow A^T(b-Ax) = 0$.
- $X$ has a unique element $x_{LS}$ having minimal 2-norm.
- $X = \{x_{LS}\} \Leftrightarrow rank(A) = M+N+1$.

The order of the system can be determined through the rank of the matrix $A$. When $A$ has full rank, there is a unique least square solution. Otherwise, there will be infinite number of solutions. The algorithm of finding the system order with given data is as follows:

1. Assume denominator order $N$ and numerator order $M$.
2. Construct matrix $A$ as in Equation (4.4) using the given data.
3. Find the rank $R$ of matrix $A$.
4. If $R < N+M+1$, it means that the assumed order is higher than needed; reduce the order until $R = N+M+1$, then the minimum order required will be found.

Since the rank of the matrix $A$ is the same as its number of nonzero singular values, the rank can be obtained by finding the number of nonzero eigenvalue of $A^H A$. In numerical solution, the minimum eigenvalue is plotted as a function of the estimated order. When there is no tremendous decrease in the minimum eigenvalue of $A^H A$, the approximation order is obtained.

Since matrix $A$ does not have the ill-conditioned problem as those matrices used in [16] and [46], there is no problem in estimating the order for systems with high orders.

Below is an example showing how the above method differs from those described in [46] and how to choose the order. Figure 4.4 compares the change of minimum eigenvalue of $A^H A$ with respect to the estimated order for both orthogonal polynomial and the ordinary power series.

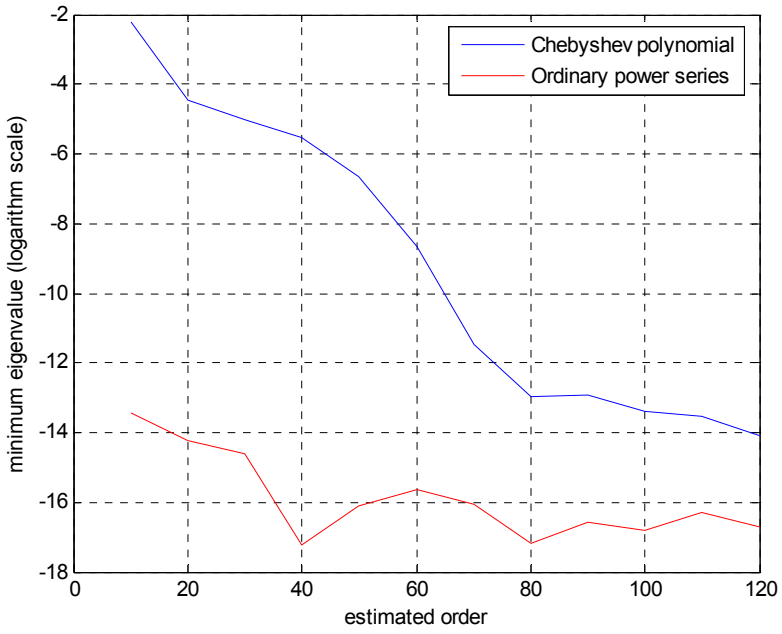


Figure 4.4 Minimum eigenvalue vs. estimated order for both orthogonal and ordinary power series.

In Figures 4.4, the dashed curve reflects the ill-conditioned problem associated with the ordinary power series. No information about the system order can be obtained from the eigenvalues of $A^H A$ as a result of the rank deficiency by the power series itself. However, the solid curve shows the case when orthogonal polynomials are involved. Figure 4.4 shows that the order is around 66 for the data given.

Figure 4.5 shows the approximation of the $S_{11}$ parameter under the order 66 using the Chebyshev of the first kind. The approximation agrees very well with the original data.

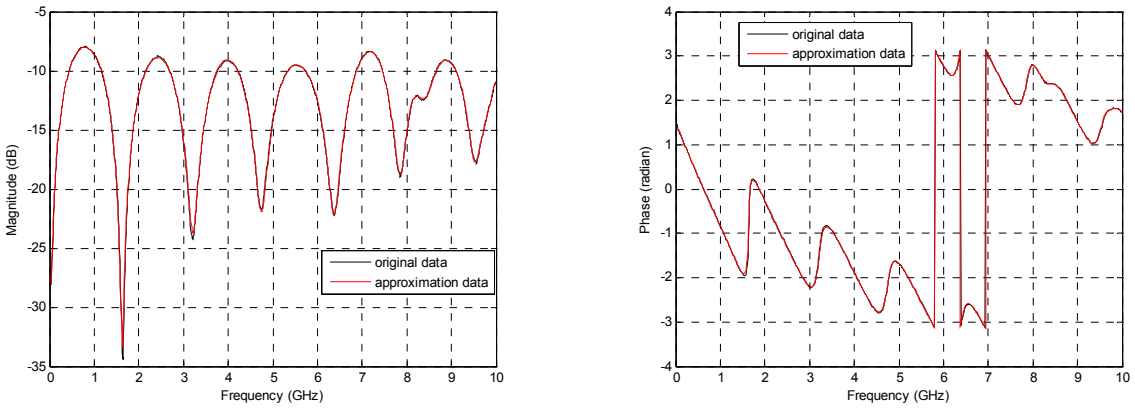


Figure 4.5 $S_{11}$ approximation with order 66.

## 4.5 Sampling Method

The data that are used to estimate the system usually come either from EM solver or from measurement. The number and positions of sampling points are important factors for the accuracy and efficiency of the approximation.

### 4.5.1 Number of sampling points

As discussed in Section 4.4, the rank of matrix $A$ is an important factor in deciding the system order and the coefficients of the system. The dimension of matrix $A$ is $K$ by $M+N+1$, where $K$ is the total sampling points. If $K$ is less than or equal to $M+N+1$, there is not enough information and no unique solution for the coefficients. Therefore, the least number of the sampling points is $M+N+1$.

### 4.5.2 Choosing the right sampling points

In the previous discussion, we assumed that there were enough data points and the information was enough for approximation. However, there are real situations when the

data points are limited. In this section, we will focus on how the sampling points influence the accuracy of the approximation and on ways to deal with insufficient data.

Lagrangian interpolation formula is applied in [54] to find the best fitting points of an order $n$ polynomial to minimize the approximation error. Based on the least square criterion, the selection of the sampling points depends on the weight function $w(x)$ of the error function $\int_{-1}^{1} w(x)e^2(x)dx$, where $e^2(x)$ is the error square at frequency point $x$. It shows in [54] that when $w(x)$=1, the best fitting points are selected to be the zeros of the $n+1$ Legendre polynomial. When $w(x) = (1-x^2)^{-1/2}$, the zeros of the $n+1$ Chebyshev polynomial will be the best matching point.

Similar to the above, the approximation using rational function also has best fitting frequency points, which minimizes the least square error. Interpolation is used to provide the unavailable data. Since the Lagrangian interpolation needs to be recomputed every time when the data is changed, Newton's interpolation formula is used to generate more data points. Define

$$f[x_0] = f(x_0)$$

$$f[x_0, x_1] = \frac{f[x_1] - f[x_0]}{x_1 - x_0}$$

$$\vdots$$

$$f[x_0, \cdots x_k] = \frac{f[x_1, \cdots x_k] - f[x_0, \cdots x_{k-1}]}{x_k - x_0}$$

and the *k*th degree interpolation polynomial will be

$$f_{x_0 \cdots x_k}(x) = f[x_0] + f[x_0, x_1](x - x_0) + \cdots + f[x_0, \cdots x_k](x - x_0) \cdots (x - x_{k-1})$$

The linear and quadratic (forward) interpolation formulae correspond to first and second order truncation respectively.

The example below shows how the sampling points affect the accuracy of the approximation. A total of 801 evenly spaced data points are given over a 5-Ghz frequency range. The magnitude and phase of the original system, as well as the approximated system based on different data sets are shown in Figure 4.6. The all-data curve use all the 801 data points for approximation. The four sampling sets sample data every four frequency points, with different starting points, respectively. Therefore, each set has 200 data points. The same order of 85 is applied to all approximations.

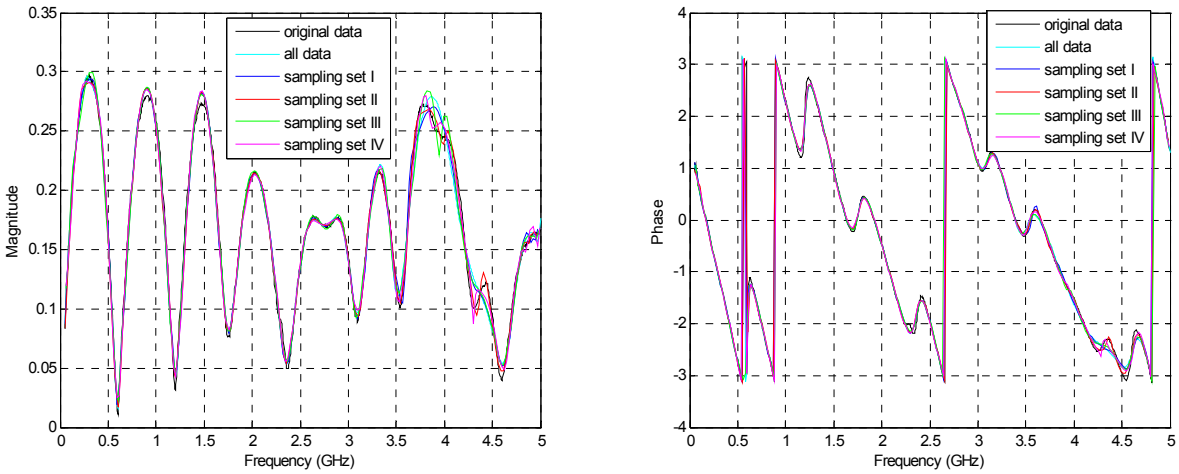


(a) (b)

Figure 4.6 Comparisons of different sampling sets. (a) Magnitude. (b) Phase of the original and approximated $S_{22}$ under different sampling sets.

Figure 4.7 shows the root mean square (RMS) error of the approximation for the different data sets with respond to frequency. Figures 4.6 and 4.7 both show that the second sampling set gives better approximations than all other sampling sets, as well as the whole data set. Therefore, it is not the number of the data points but their location that is important.

The selection of the sampling points reduces the total number of data that can be used in the approximation. In order to have enough sampling points, satisfying $K \gg M + N + 1$, the second-order interpolation method described is applied.

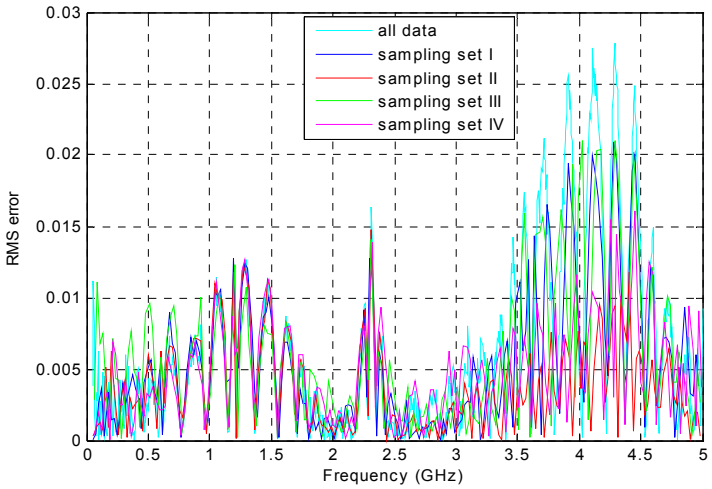


Figure 4.7 Comparisons of RMS error of the $S_{22}$ for different sampling sets.

## 4.6 Numerical Results

To demonstrate the efficiency of the orthogonal polynomials, different cases are investigated in this chapter.

### 4.6.1 Case study I – Comparison of the power series with orthogonal polynomials

The scattering parameters of an interconnect system with V-shaped cross section measured over 10 GHz are used as an example to demonstrate the accuracy and validity of the proposed method. The example has a very complex frequency-domain behavior that can be extremely difficult to approximate using the standard power series polynomial. The insertion loss of the interconnect is approximated using the power series, Legendre, and Chebyshev of the first and second kinds as shown in Figures 4.8(a) and

(b). All three orthogonal series show superior accuracy when compared to the standard power series approximation.

Figure 4.9 shows that the approximation using standard power series has a larger deviation from the original data. The accuracy improvement of the orthogonal polynomial is attributed to the improved numerical stability of the interpolation matrix.

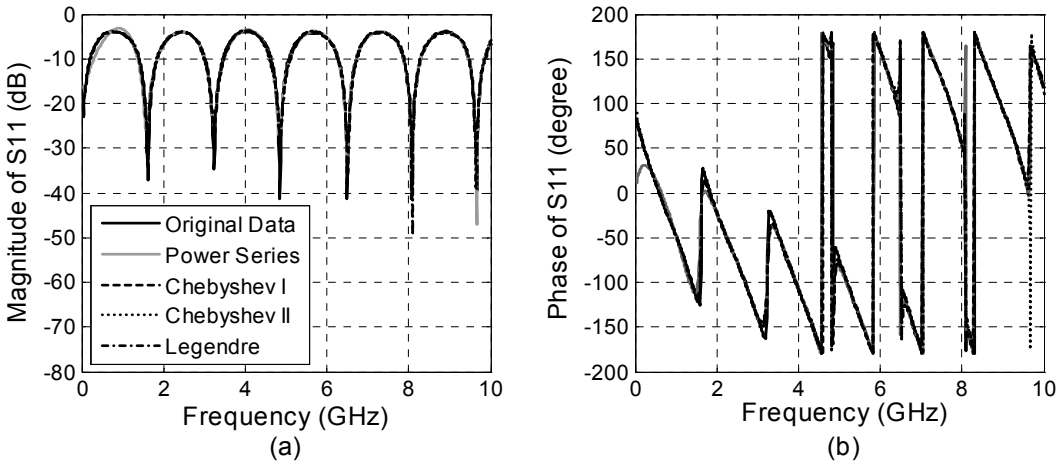


Figure 4.8 Comparisons of the power series and the classical orthogonal polynomials. (a) Magnitude. (b) Phase of the original and approximated $S_{11}$.

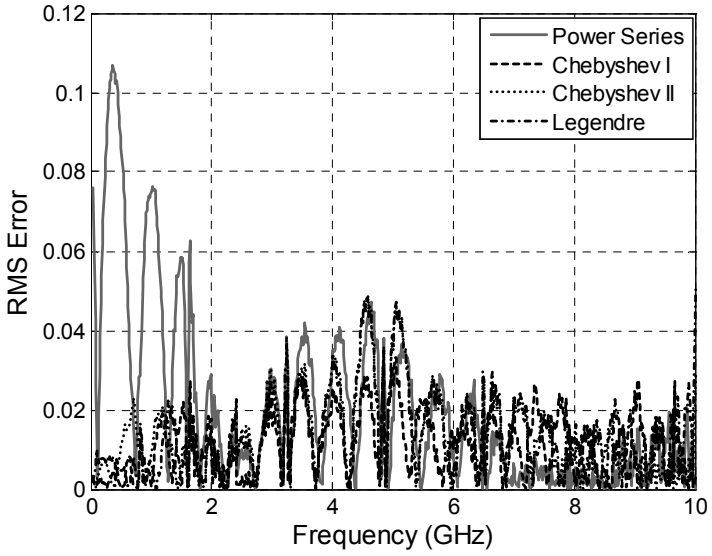


Figure 4.9 Comparisons of the RMS error for the 40-order $S_{11}$ approximation.

Figure 4.10 shows that the condition number of the power series polynomial increases superlinearly with the order of the approximation, until it approaches the floating-point relative accuracy. However, the condition number of the orthogonal polynomials remains almost flat as the order of approximation increases.

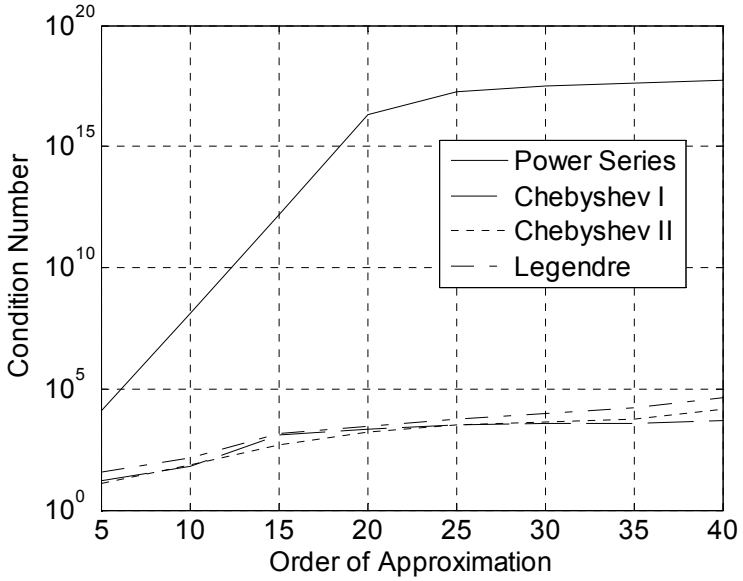


Figure 4.10 Comparisons of the condition number of the polynomials as a function of approximation order.

Once the frequency-domain approximation is obtained, recursive convolution can be applied to predict the time-domain response.

### 4.6.2 Case study II – Four-port system by different orthogonal polynomials

The example in Section 4.6.1 focuses on comparing the orthogonal polynomials with the ordinary power series. The result shows a much better approximation through the orthogonal polynomials. In this section, we will compare the three orthogonal polynomials to see the difference.

This example shows a case when the scattering parameter of a four-port system is given in the real and imaginary form. The poles of the system can be approximated by

one of its parameters. Here we use the $S_{12}$ data. After the poles are extracted from $S_{12}$, we will obtain the residues for all other parameters, respectively. Three orthogonal polynomials are applied with the same order (order 22), and the simulation results are compared. Figure 4.11 compares the root mean square error of the three kinds of orthogonal polynomials for the $S$ parameters. Because of the symmetric property, $S_{ij}$ is the same as $S_{ji}$. Therefore, only one of the two parameters is plotted.

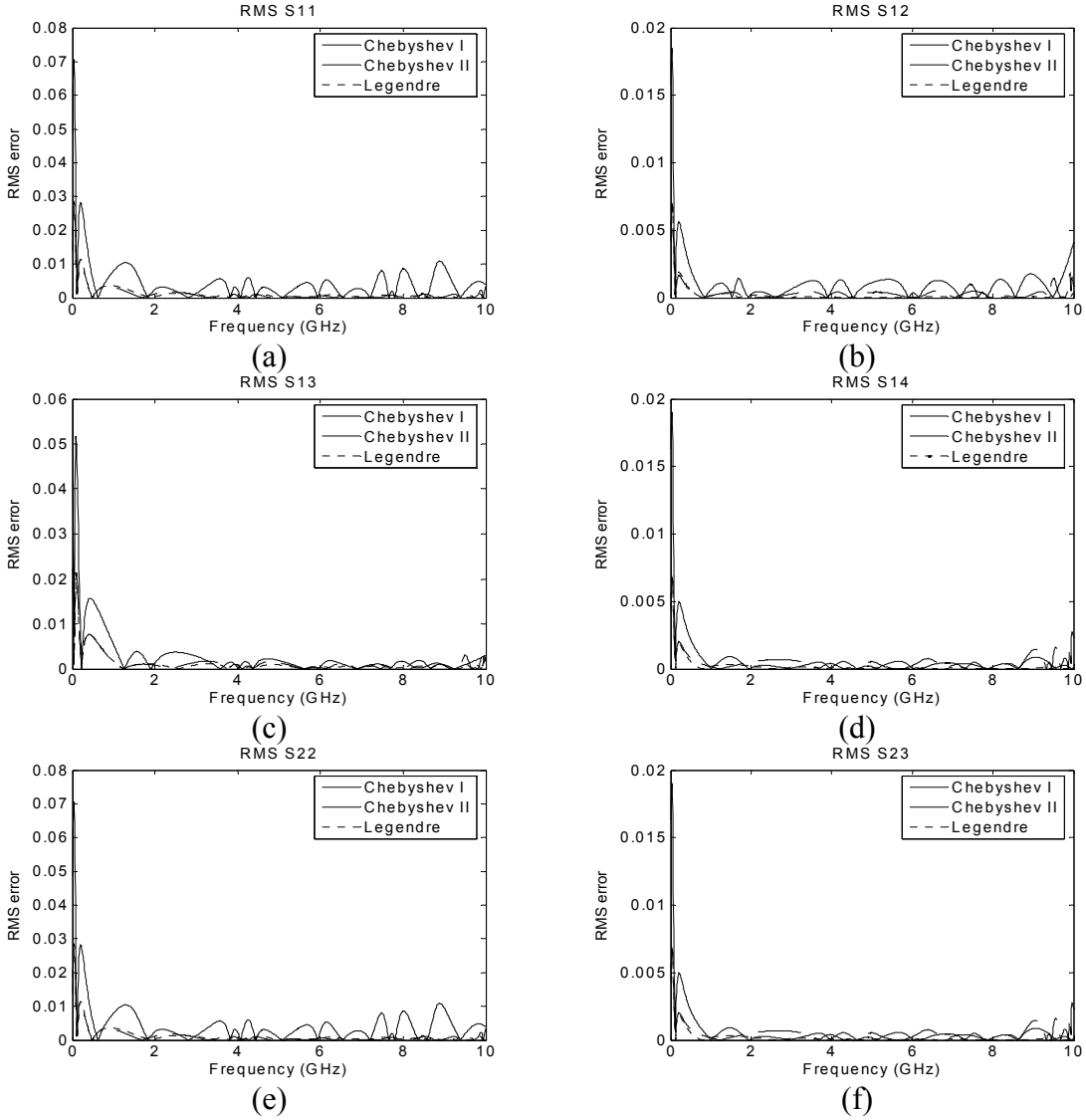


Figure 4.11 Comparison of RMS error for different polynomials with the same approximation order.

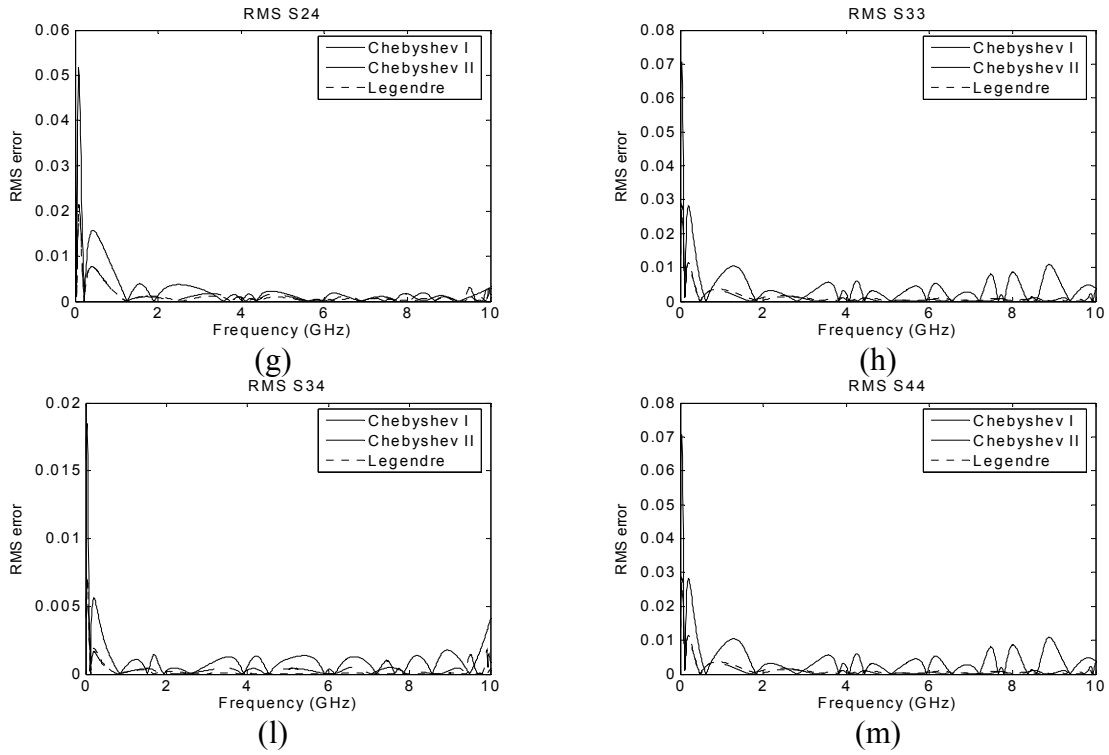


Figure 4.11 Continued.

From the above figures, it is obvious that the Chebyshev polynomial of the first kind gives the worst approximation over the whole frequency range for all parameters. For parameters such as $S_{ii}$, $(i = 1, \cdots, 4)$, the Chebyshev of the second kind and the Legendre polynomials have almost the same order of error except at the high frequency end. For all other parameters, the Legendre polynomials gives better approximation over the whole frequency range. As a result, the Legendre polynomial gives the best approximation for this case.

Figure 4.12 is the plot and number of poles obtained from the three orthogonal polynomials. Using the same approximation order of 22 and solve for the poles of the system by different polynomials, the Chebyshev polynomials of the first and second kind approximate the system with 18 and 21 poles, respectively. The number of poles is less than the original assumed 22, which is because the poles on the imaginary axis are

removed for stability reason. For Legendre polynomial, the 22 poles are all located in the left half plane and are kept.

The above result shows that, for a given set of data, the accuracy of the approximation depends on the type of orthogonal polynomials applied. The result explains from the other view that the locations of the sampling points are important in determining the approximation accuracy. Instead of applying the same kind of polynomial and changing the sample points, the same sample points are fitted with different types of polynomials. The difference in the characteristic of each polynomial asks for different sampling data for the best accuracy.

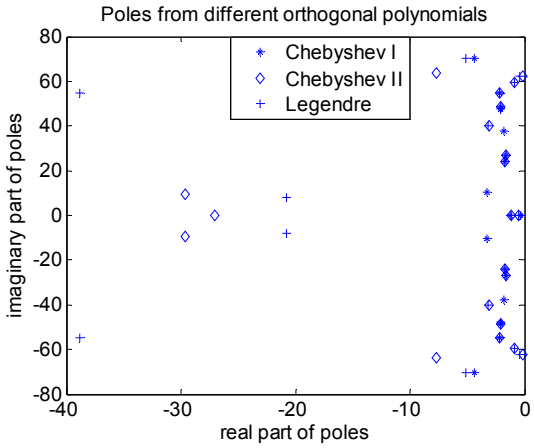


Number of poles:

Chebyshev I: 18

Chebyshev II: 21

Legendre: 22

Figure 4.12 Location and number of poles for different polynomials.

## 4.7 Recursive Convolution

From above discussions, we can successfully approximate a system characterized by tabulated frequency domain data by a ration function $H(s)$. The output of the system for a given input $X(s)$ is $Y(s) = H(s)X(s)$ in the frequency domain. The time domain response of the system is the inverse Laplace transform of $Y(s)$. However, since $H(s)$

obtained above is in the form of rational function, the more efficient recursive convolution can be applied to find the time domain response of the system.

Recursive convolution was first discussed in [55]. Later, the efficiency of the recursive convolution was further shown in [56], [57] for its application in transient analysis of transmission line.

### 4.7.1 Recursive convolution algorithm

For systems characterized by rational functions, system response in frequency domain is expressed as

$$H(s) = k_0 + \sum_{i=1}^{N} \frac{k_i}{s + p_i} \tag{4.13}$$

All the poles and residues of $H(s)$ are obtained from the discussion above. For the direct term, its corresponding time domain response is an impulse. For each frequency-dependent term, the corresponding time domain response is an exponential term. Since the system is stable, the exponential terms are decaying as time increases. The time domain response is real due to the enforcement of poles are either real or in complex conjugate pair.

Recursive convolution for one term in the summation is derived. The corresponding time domain response for $\frac{k_i}{s + p_i}$ is $k_i e^{-p_i t}$. Convolved with input $x(t)$, we have,

$$y_i(t) = k_i e^{-p_i t} * x(t) \tag{4.14}$$

where

$$y_i(t) = \int_0^t k_i e^{-p_i \tau} x(t-\tau) d\tau = \underbrace{\int_0^h k_i e^{-p_i \tau} x(t-\tau) d\tau}_{I_1} + \underbrace{\int_h^t k_i e^{-p_i \tau} x(t-\tau) d\tau}_{I_2} \tag{4.15}$$

and $h$ is the time step. In the second integral, set $\tau = \tau' + h$ which implies $\tau' = \tau - h$

$$I_2 = \int_0^{t-h} k_i e^{-p_i(\tau'+h)} x(t-\tau'-h) d\tau' = e^{-p_i h} \int_0^{t-h} k_i e^{-p_i \tau'} x(t-\tau'-h) d\tau' \tag{4.16}$$

Therefore $I_2 = e^{-p_i h} y_i(t-h)$ and

$$y_i(t) = \underbrace{\int_0^h k_i e^{-p_i \tau} x(t-\tau) d\tau}_{I_1} + e^{-p_i h} y_i(t-h) \tag{4.17}$$

Evaluating $I_1$

$$I_1 = k_i x(t-h) \int_0^h e^{-p_i \tau} d\tau \tag{4.18}$$

where we assume a step invariant (constant) behavior of the input function. This can be evaluated to yield

$$I_1 = \frac{k_i x(t-h)}{p_i} \left(1 - e^{-p_i h}\right) \tag{4.19}$$

So that

$$y_i(t) = \frac{k_i x(t-h)}{p_i} \left(1 - e^{-p_i h}\right) + e^{-p_i h} y_i(t-h) \tag{4.20}$$

Which is the *recursive convolution* formula for a step-invariant approximation for each time in the transfer function.

Therefore, the complete solution for $y(t)$ at each time step is

$$y(t) = k_0 x(t-h) + \sum_{i=1}^{N} y_i(t) \tag{4.21}$$

where $y_i(t)$ is given in Equation (4.20).

### 4.7.2 Transient response for systems characterized by scattering parameter

Figure 4.13 shows a black box system characterized by its scattering parameter matrix. The excitation and termination are given as well.

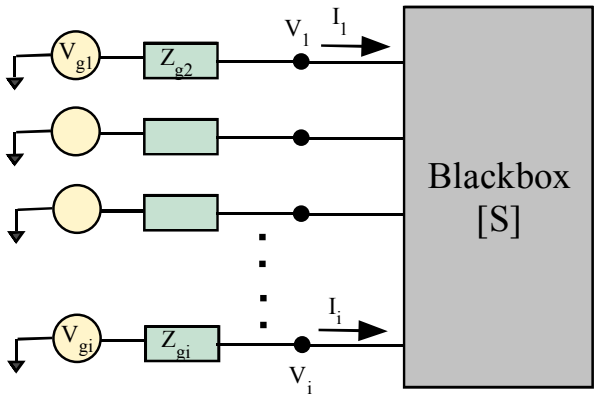


Figure 4.13 Black box characterized by scattering matrix.

Assume the scattering matrix is represented by $H(s)$, the input and output to the black box are $X(s)$ and $Y(s)$, respectively. In time domain, the *N*-Port *S*-parameter equation is

$$y(t) = h(t) * x(t)$$

The termination condition is

$$y(t) = \Gamma(t)x(t) + T(t)V_g(t)$$

where $\Gamma(t)$ is the reflection coefficient matrix, $T(t)$ is the voltage division matrix, and $V_g(t)$ is the source voltage vector.

$$\Gamma(t) = -[I + Z_T Z_0^{-1}]^{-1}[I - Z_T Z_0^{-1}]$$

$$T(t) = [I + Z_T Z_0^{-1}]^{-1}$$

$Z_T$ is the termination impedance matrix and $Z_0$ is the reference impedance matrix. Voltage $V(t)$ is the summation of $y(t)$ and $x(t)$.

### 4.7.3 Numerical results

This example shows the simulation results for a two-port RLC network as in Figure 4.14. The value of the resistance, inductance, and capacitance are $R = 50\ \Omega$, $L = 1$ nH, and $C = 1$ pF. The scattering parameter matrix of the network is calculated from DC to 250 GHz.

First, rational function approximation is performed to construct the system model. Poles and residues obtained from the approximation are list in Table 4.2.

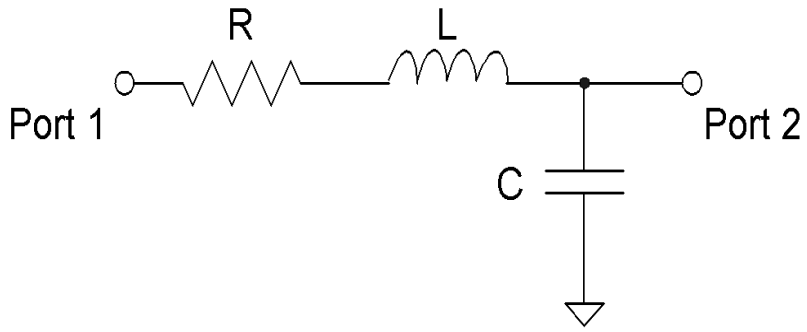


Figure 4.14 Two-port RLC network.

Table 4.2: RLC network poles and residues from approximation

| Poles | $S_{11}$ | $S_{12}$ | $S_{21}$ | $S_{22}$ |
|---|---|---|---|---|
| | 0.9998 | -0.0004 | -0.0004 | -1.0006 |
| -85.0417 | -128.4076 | -36.9569 | -36.9569 | -7.7681 |
| -33.6216 | 28.6102 | 37.4286 | 37.4286 | 48.4417 |

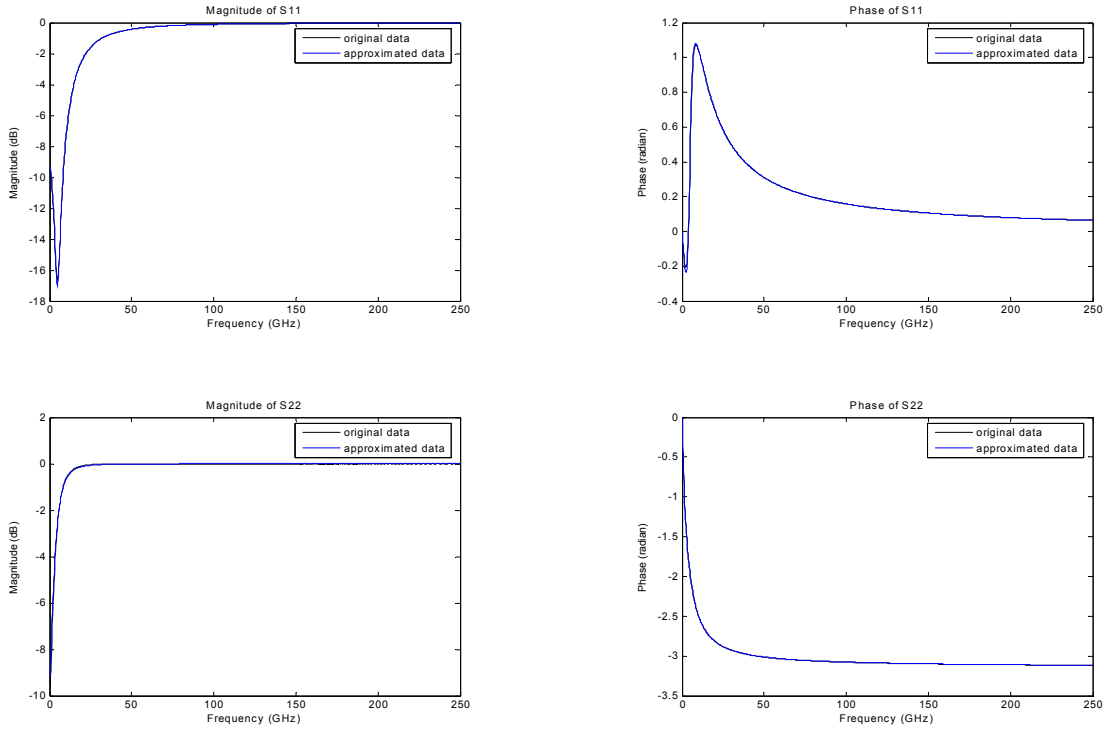


Figure 4.15 Magnitude and phase approximation for the RLC network.

Figure 4.15 shows the approximation of magnitude and phase for parameters $S_{11}$ and $S_{22}$. Good agreements are shown between the original and approximated data in the frequency domain.

Once the poles and residues are obtained from approximation, time domain response of the system can be calculated through recursive convolution.

The reference impedance matrix is $Z_0 = \begin{bmatrix} 50 & 0 \\ 0 & 50 \end{bmatrix}$, and the termination matrix is $Z_T = \begin{bmatrix} 50 & 0 \\ 0 & 50000 \end{bmatrix}$. There is no excitation at port 2. At port one, the excitation is a pulse with magnitude one, rise and fall time 0.0102 ns, and width 1.0230 ns. The time domain

response of the system is shown in Figure 4.16. The solid line is the response at port one, while the dash line is the response at port two.

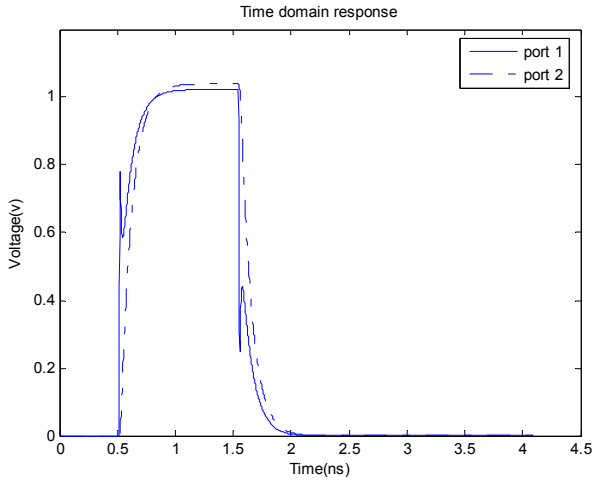


Figure 4.16 Time domain response for the RLC network.

## 4.8 Conclusion

An efficient macromodeling method is presented to approximate frequency response of a black-box system. The utilization of orthogonal polynomials overcomes the ill-conditioning problem and hence improves the modeling accuracy. The stability and causality of the macromodel is guaranteed inherently. The model order estimation and sampling scheme improves both efficiency and accuracy of modeling. Recursive convolution is applied to find the time domain response once the approximation is done.

# 5 PASSIVE MACROMODELS

## 5.1 Introduction

In Chapter 4, rational function approximation via orthogonal polynomials is presented. An accurate transfer function model can be obtained from measured data or computational results of full-wave simulations for multiport network. The macromodel constructed satisfies all other requirements of a physically real system except the passivity criterion. Unlike the case in MOR where provided that the original state-space model is passive, the resultant reduced order system can be guaranteed to be passive by some methods such as PRIMA [27] and the method proposed in [31], etc. None of the existing curve fitting methods can assure passivity of the resultant macromodels even if the original frequency data is passive.

If passivity of the real system is not preserved, the macromodel cannot be used in subsequent time domain simulations. The reason is because nonpassive networks can produce unbounded outputs under certain termination conditions. Therefore, preserving passivity in the resultant macromodels is an important issue for interconnect and package modeling.

The conditions for passivity have different expressions depending on whether the transfer matrix represents an admittance, impedance, hybrid, or scattering matrix. For all these cases, the condition can be expressed in terms of either eigenvalues or singular values of the transfer matrix. Hence, theoretically, the passivity criterion can be explicitly expressed and incorporated in the curve fitting procedure as a constraint. Thus, the curve-fitting problem can be formulated as a constrained optimization problem, with the error

between the desired and constructed transfer functions being the target function to optimize with and the passivity condition being the constraint. However, most of the existing optimization algorithm cannot handle this kind of problem efficiently.

Therefore, all existing passivity enforcement methods for curve fitting are a posteriori approaches based on perturbation theory. That is, a transfer matrix is obtained first without taking the passivity into account. Then the macromodel is adjusted by various compensation methods to enforce passivity, assuming only weak violation of passivity in the original macromodel.

In this chapter various expressions of the passivity condition are first briefly discussed. Then different approaches to enforce passivity are described and compared.

## 5.2 Passivity Definitions

### 5.2.1 Admittance and impedance matrices

When $H(s = j\omega)$ is the admittance matrix of a multiport network, we have

$$i = H(j\omega)v \tag{5.1}$$

where $i$ and $v$ are the port current and port voltage vectors, respectively. The reference direction for $i$ is the direction flowing into the network. The power that the network consumes is $P = \mathrm{Re}[v^H(j\omega)i(j\omega)]$[61]. Hence, the network is passive if and only if the following inequality holds [41], [42]:

$$\mathrm{Re}[v^H(j\omega)i(j\omega)] \geq 0, \text{ for any } \omega \tag{5.2}$$

where the superscript H is the complex conjugate transpose or Hermitian operator. Replacing $i(j\omega)$ in Equation (5.2) by Equation (5.1), we will have,

$$
\begin{aligned}
&\mathrm{Re}[v^H H(j\omega)v] \\
&= \frac{1}{2}\left(v^H H(j\omega)v + [v^H H(j\omega)v]^*\right) \\
&= \frac{1}{2}\left(v^H H(j\omega)v + v^T H^*(j\omega)v^*\right) \\
&= \frac{1}{2}\left(v^H H(j\omega)v + v^H H^H(j\omega)v\right) \\
&= \frac{1}{2} v^H \left(H(j\omega) + H^H(j\omega)\right) v \geq 0
\end{aligned}
\tag{5.3}
$$

where the superscripts $T$ and * are respectively the transpose and complex conjugate operators. Hence, the passivity condition for the admittance matrix is

$$
v^H \left(H(j\omega) + H^H(j\omega)\right) v \geq 0 \tag{5.4}
$$

for an arbitrary vector $v$ and at any frequency $\omega$. For reciprocal networks, $H(j\omega)$ is symmetric, and thus we have

$$
H(j\omega) + H^H(j\omega) = H(j\omega) + H^*(j\omega) = 2\,\mathrm{Re}[H(j\omega)] \tag{5.5}
$$

Therefore, the passivity condition for symmetric $H(j\omega)$ is that $\mathrm{Re}[H(j\omega)]$ is positive semidefinite [41], [42]. That is,

$$
\lambda_i(j\omega) \geq 0 \quad \forall \lambda_i(j\omega) \in \lambda(\mathrm{Re}[H(j\omega)]) \quad \forall \omega \tag{5.6}
$$

where $\lambda(Z)$ is the set of eigenvalues of $Z$. It is easy to derive that the passivity condition for the impedance and hybrid matrices is the same as (5.6).

### 5.2.2 Scattering matrix

When $H(s = j\omega)$ is the scattering matrix of a multiport network, we have

$$
b = H(j\omega)a \tag{5.7}
$$

where $a$ and $b$, respectively, are the incoming and outgoing signal vectors. The power that the network consumes is $P = a^H(j\omega)a(j\omega) - b^H(j\omega)b(j\omega)$. Hence, the network is passive if and only if the following inequality holds [41], [42].

$$a^H(j\omega)a(j\omega) - b^H(j\omega)b(j\omega) \geq 0, \text{ for any } \omega \tag{5.8}$$

Using (5.7), (5.8) can be written as

$$\begin{aligned} & a^H a - b^H b \\ &= a^H a - a^H H^H H a \\ &= a^H \left( I - H^H H \right) a \geq 0 \end{aligned}$$

Hence, the passivity condition for the scattering matrix is

$$a^H \left( I - H^H(j\omega)H(j\omega) \right) a \geq 0 \tag{5.9}$$

for an arbitrary vector $a$ and at any frequency $\omega$. $H(j\omega)$ that satisfies this condition is unitary bounded, which is equivalent to

$$\max_{i,\omega} \sigma_i(j\omega) \leq 1 \quad \forall \sigma_i(j\omega) \in \sigma(H(j\omega)) \tag{5.10}$$

where $\sigma(H(j\omega))$ is the set of singular values of $H(j\omega)$ and $\sigma_i(j\omega)$ is the *i*th singular value, which is defined as

$$\sigma_i \geq 0 \in \sigma(H) \Leftrightarrow \sigma_i^2 \in \lambda(H^H H)$$

### 5.2.3 A sufficient condition

A sufficient condition for constructing a passive network is based on the fact that the summation of passive subnetworks is also passive. As given in [16], a rational transfer matrix $H(s)$ of a multiport network can be expressed as

$$H(s) = \sum_{m=1}^{LPN} \frac{\gamma_m}{s - p_{mr}} + \sum_{n=1}^{BPN} \frac{2\alpha_n (s - p_{nr}) - 2\beta_n p_{ni}}{(s - p_{nr})^2 + p_{ni}^2} + \sum_{k=1}^{HPN} \frac{\psi_k s}{s - p_{kr}} + \delta + \eta s \tag{5.11}$$

where the first term corresponds to a low-pass filter, the second a band-pass filter, the third a high-pass filter, and the last two terms correspond to an all-pass filter. All the coefficients written in boldface are $N_p \times N_p$ matrices, where $N_p$ is the number of ports of the network. All parameters in the above equation are real.

A sufficient condition for $H(s)$ to be passive is that each of the filter in (5.11) is passive [16]. Assuming $H(s)$ is an admittance, impedance, or hybrid matrix, the passivity of all the filters in (5.11) are characterized by their real parts for $s = j\omega$. The real part of (5.11) can be written as

$$\mathrm{Re}[H(jw)] = \sum_{m=1}^{LPN} \frac{-\gamma_m p_{mr}}{\omega^2 + p_{mr}^2} + \sum_{n=1}^{BPN} \frac{2\omega^2(-\alpha_n p_{nr} + \beta_n p_{ni})}{(p_{nr}^2 + p_{ni}^2 - \omega^2)^2 + (2p_{nr}\omega)^2}$$
$$+ \sum_{n=1}^{BPN} \frac{2(p_{nr}^2 + p_{ni}^2)(-\alpha_n p_{nr} - \beta_n p_{ni})}{(p_{nr}^2 + p_{ni}^2 - \omega^2)^2 + (2p_{nr}\omega)^2} + \sum_{k=1}^{HPN} \frac{\psi_k \omega^2}{\omega^2 + p_{kr}^2} + \delta$$

The condition for each of the filters to be passive is that matrices $\gamma_m$, $-\alpha_n p_{nr} \pm \beta_n p_{ni}$, $\psi_k$ are all positive semidefinite; that is, their eigenvalues are not less than zero.

## 5.3 Passivity Enforcement

### 5.3.1 Passive filter approach

Based on the aforementioned sufficient condition, a simple approach to enforce passivity is to modify the coefficient matrices in (5.11) to assure that each individual filter term is passive [16]. First, the eigenvalues of the coefficient matrices are computed.

Then negative eigenvalues are picked out as target eigenvalues to modify. Perturbation theory of the matrix spectrum is used to drive the target eigenvalues to nonnegative values, so that the macromodel becomes passive.

The advantage of this approach is that the coefficient matrices are frequency independent. Therefore, once the passivity requirement is achieved, the macromodel is guaranteed to be globally passive. The disadvantage of this method is that the condition required is sufficient but necessary. Each term in the macromodel being passive is not a necessary condition for the entire macromodel to be passive. Accuracy in transfer function approximation may be sacrificed for this overly conservative passivity enforcement condition.

### 5.3.2 Quadratic programming approach

A passivity enforcement approach using quadratic programming is presented in [24]. Same as in the passive filter approach, passivity is enforced by modifying the coefficients of an existing rational transfer function. Meanwhile, the mean square error between the modified transfer function and the target curve is also minimized. This approach is described briefly below.

Assume $Y_{fit}(s)$ is the rational approximation of a target transfer matrix $Y(s)$ and its $(i, j)$th element can be expressed as

$$Y_{fit(i,j)}(s) = \sum_{m=1}^{N} \frac{c_m}{s - a_m} + d + se \tag{5.12}$$

Since $Y_{fit}(s)$ can be nonpassive, the goal is to modify coefficients $a_m$, $c_m$, $d$, and $e$ to enforce the passivity, i.e., to insure that $G_{fit}(s) = \mathrm{Re}[Y_{fit}(s)]$ is positive semidefinite.

The columns of $Y_{fit}(s)$ are stacked into a single vector $y_{fit}$ and all the coefficients that need to be modified are stacked into another single vector $x$. An incremental relationship between the changes in $y_{fit}$ and $x$ can be obtained by the linearization of the above equation:

$$\Delta y_{fit} = M\Delta x \tag{5.13}$$

Taking the real part of the above equation yields

$$\Delta g_{fit} = \mathrm{Re}[M]\Delta x = P\Delta x \tag{5.14}$$

where $g_{fit}$ is a single vector that holds all the columns of $G_{fit}(s)$. Using the perturbation theory of eigenvalues, the relationship between the change in the eigenvalues of $G_{fit}(s)$ and $\Delta g_{fit}$ can be obtained

$$\Delta\lambda = Q\Delta g_{fit} \tag{5.15}$$

Therefore, we have

$$\Delta\lambda = Q\Delta g_{fit} = QP\Delta x = R\Delta x \tag{5.16}$$

Thus, the problem to solve is to find $\Delta x$ such that

$$\begin{aligned} &y(s) - (y^0_{fit}(s) + M\Delta x) \to 0 \\ &\Delta\lambda = R\Delta x \geq -\lambda_0 \end{aligned} \tag{5.17}$$

To find the least mean square solution, this problem can be formulated as a constrained quadratic programming problem as follows:

Minimize

$$\frac{1}{2}\Delta x^T H \Delta x - f^T \Delta x \tag{5.18}$$

with the constraint

$$R\Delta x \geq -\lambda_0$$

where

$$H = M^T M \text{ and } f = M^T (y - y_{fit}^0) \tag{5.19}$$

By solving the constrained equation in (5.18), the perturbations needed for each parameter will be obtained and the passivity of the macromodel is guaranteed.

### 5.3.3 Hamiltonian matrix approach

Another approach is presented in [25], [26] and based on the Hamiltonian matrix. The idea is to locate the frequency bands where passivity is violated by checking the imaginary eigenvalues of the Hamiltonian matrix. Then an iterative perturbation scheme is developed to compensate the violations.

A time-invariant multiport system expressed in state-space form is considered.

$$\begin{aligned} \dot{x}(t) &= Ax(t) + Bu(t) \\ y(t) &= Cx(t) + Du(t) \end{aligned} \tag{5.20}$$

The transfer matrix is

$$H(s) = D + C(sI - A)^{-1} B \tag{5.21}$$

When $H(s)$ is the scattering matrix, the passivity violation detection is based on the following theorem.

Assume that $A$ has no imaginary eigenvalues, $\gamma > 0$ is not a singular value of $D$, and $\omega_0$ is a real number. Then, $\gamma \in \sigma(H(j\omega_0))$ if and only if $j\omega_0 \in \lambda(M_\gamma)$, where

$$M_\gamma = \begin{pmatrix} A - BR^{-1}D^T C & -\gamma BR^{-1}B^T \\ \gamma C^T S^{-1} C & -A^T + C^T DR^{-1}B^T \end{pmatrix} \tag{5.22}$$

$$\text{and } R = D^T D - \gamma^2 I,\ S = DD^T - \gamma^2 I \tag{5.23}$$

$M_\gamma$ is a Hamiltonian matrix. This theorem allows one to compute the frequencies where the singular values cross or touch any given threshold.

Similarly, another theorem for the hybrid matrix is given as follows:

Assume that $A$ has no imaginary eigenvalues, $\sigma > 0$ is not an eigenvalue of $(D + D^T)/2$, and $\omega_0$ is a real number. Then, $\sigma \in \lambda(G(j\omega_0))$ if and only if $j\omega_0 \in \lambda(N_\sigma)$, where

$$N_\sigma = \begin{pmatrix} A + BQ^{-1}C & BQ^{-1}B^T \\ -C^T Q^{-1} C & -A^T - C^T Q^{-1} B^T \end{pmatrix} \tag{5.24}$$

and

$$Q = 2\sigma I - D^T - D \tag{5.25}$$

After the frequency bands with passivity violation are determined, an iterative procedure is applied to modify matrix $C$ to enforce passivity. Modifying $C$ is not the only choice but is the only case investigated in [25]. A relationship is developed between $dC$, and the change of eigenvalues of $M_\gamma$ or $N_\sigma$. $dC$ is calculated to perturb the eigenvalues and meanwhile to minimize the change of $y(t)$.

## 5.4 Numerical Results

The example below shows the passivity enforcement for the case described in Section 4.6.1. After the poles of the system are extracted, the passivity-checking method described above is applied. For this illustration, the admittance matrix of the interconnect is measured and approximated using the pole-residue model. The result of the magnitude and phase before enforcing passivity are shown in Figure 5.1(a) and (b), respectively.

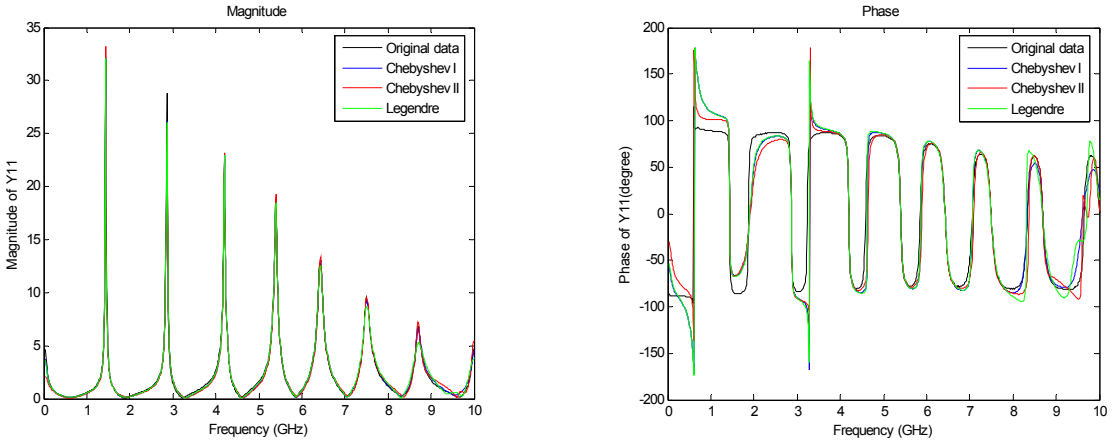


(a) (b)

Figure 5.1 The original and approximated $Y_{11}$ before applying the passivity check. (a) Magnitude plot of $Y_{11}$. (b) Phase plot of $Y_{11}$.

Then the method described in [16] is applied to check and enforce passivity to the resulting approximation. The residues and the constants are calculated by considering passivity criteria. The magnitude and phase of the passive rational model are shown in Figure 5.2(a) and (b), respectively.

Since the method described in [16] is a sufficient but not necessary condition of passivity enforcement, we would expect less accuracy for the approximation with passivity check. Comparing the plots in Figures 5.1 and 5.2, it is obvious that the passivity enforcement method sacrifices the accuracy of the approximation.

The quadratic programming approach will be the most accurate one. However, it is computational expensive and cannot be applied to large problems.

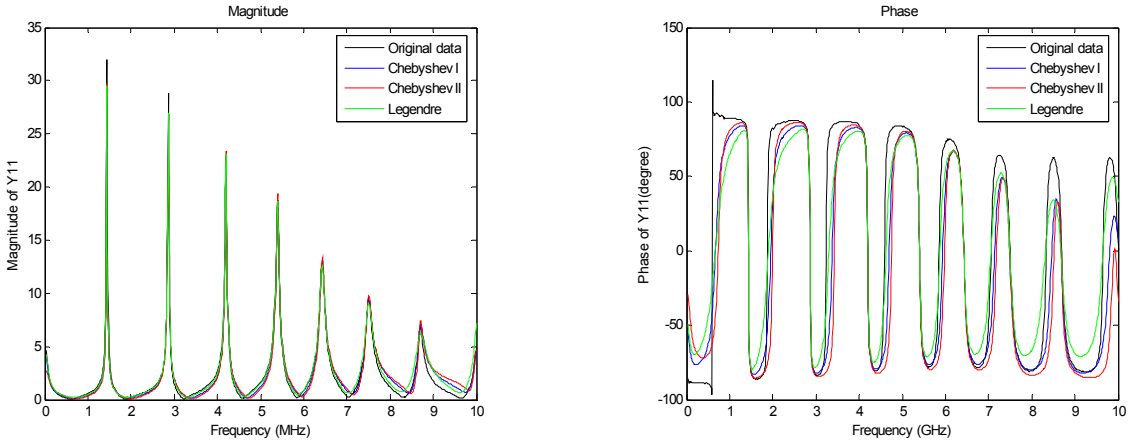


(a) (b)

Figure 5.2 The original and approximated $Y_{11}$ after applying the passivity check. (a) Magnitude plot of $Y_{11}$. (b) Phase plot of $Y_{11}$.

## 5.5 Conclusion

The existing passivity enforcement methods are generally efficient for weak violation of passivity. The passive filter approach is easy to implement and can globally assure passivity, but the accuracy of the macromodel may be compromised. The quadratic programming approach can handle relatively large passivity violations and the macromodel accuracy is optimized. However, it is computationally expensive and cannot apply to systems with order higher than 12 at present. The Hamiltonian approach is good in that the frequency bands where passivity is violated can be located. Thus, intensive frequency sampling is avoided and the macromodel accuracy is optimized; however, as noted, the approach can only handle weak passivity violations.

# 6 DATA PREPROCESSING

## 6.1 Introduction

In previous chapters, we have discussed methods to construct an accurate macromodel that has the properties of a physically real system. All the approximation is based on the frequency domain sampled data, which directly comes either from electromagnetic simulation or from microwave measurements. For all previous discussion, we assume that there are no errors with the data and use the data without any process. However, for those data obtained from electromagnetic simulations, there are numerical errors, and there is no guarantee that the data is causal and passive. For microwave measurements, noise is unavoidable; thus, the data may be neither causal nor passive.

Since the approximation is based on the original frequency data, it is obvious that the approximated system will not be causal and passive if the starting data is not causal and passive. Therefore, it is important to check and process the data for any causal and passivity violation. The noisy data also need to be processed before approximation to reduce the noise effect.

## 6.2 Noise Filtering

In cases where the data is very noisy, the approximation can be tedious and involve much higher orders than necessary. Therefore, it is very important to preprocess the data to reduce the influence of the noise during the approximation.

To facilitate discussions within this section, it should be noted that the terms *noise frequency*, *white noise*, and *colored noise* etc. all refer to the Fourier domain of the raw data under preprocessing instead of referring to the physical frequency domain.

The noise from measurements can either be white or colored noise. The white noise is random noise that spreads the whole frequency band and has a homogeneously distributed power spectrum across all frequencies [38], i.e., $\phi(j\omega) = \sigma^2$ for all frequency $\omega$, where $\phi(j\omega)$ is the power spectrum and $\sigma$ is a constant. The white noise is uncorrelated and characterizes random variations during the measurements.

Different from the white noise, the colored noise is correlated and does not have a uniform power spectrum. Based on the noise characteristics, different types of filters can be applied to remove colored noise. Kalman filters, when carefully designed, can significantly improve the signal-to-noise ratio (SNR) of colored noise.

For white noise, filtering mainly deals with the random variations in the measurements. The most straightforward approach consists of applying the moving average filter. The goal is to cancel or reduce the random noise effect in the measurement data. Assume the original data sequence is $h[n]$, an $(M_1 + M_2 + 1)$th order moving average filter calculates the *n*th data $\overline{h}[n]$ as [38]:

$$\overline{h}[n] = \frac{1}{M_1 + M_2 + 1} \sum_{k=-M_1}^{M_2} h[n-k]$$

With the application of the moving average filter, the measurement data can be improved. Figure 6.1 shows the difference between the original noise measurement data and the data filtered with a ninth-order moving average filter. Comparing the original

data in the solid curve and the filtered data in the dashed curve, it is obvious that the filter removes some of the random noise and will make the approximation much easier.

In the above moving average filter, all the data around $n$ are equally weighted in evaluating the filtered value of $\bar{h}[n]$. By considering the fact that the most recent data tend to have greater impact on the evaluation point, different weights can be applied to different data points. Therefore, improvement can be made by using the exponentially weighted moving average filter.

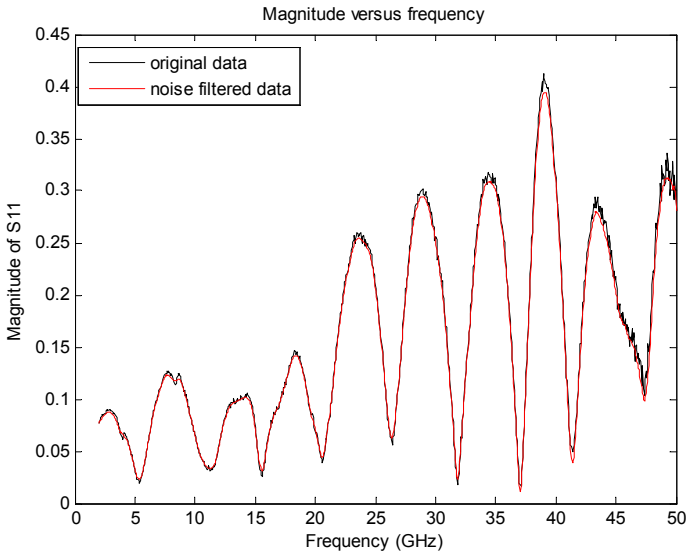


Figure 6.1 Improving noisy data with moving average filter.

Besides the commonly used moving average filter, filters based on local fitting are also widely used. The locally weighted scatter plot smoothing (LOWESS) [58], and the local polynomial regression fitting (LOESS) [59]. The idea of the LOWESS and LOESS methods is to smooth the data based on the local polynomial fitting.

## 6.3 Passivity Check and Enforcement

Although random noise can be neglected for the simulated data, passivity violation is a big concern for the data obtained from electromagnetic simulation. It is primarily due

to discretization or round-off error [37]. When the original data does not meet the passivity requirement at certain frequency points, a slight perturbation can be applied.

As passivity enforcement is always applied for the macromodel that approximates the system characterized by the sampled data, the need for passivity check of the original data may not seem necessary at first glance. However, passivity enforcement of the original data is important as well. The reasons to check and enforce the passivity of the original data are (a) to guarantee the convergence of the transient analysis when inverse Fourier transform is applied directly, and (b) to save time and effort in enforcing the passivity of the macromodel [60].

Despite inefficiency and time-consuming native of the inverse Fourier transform, it is still used sometimes because of its convenience, especially when the frequency bands are not too wide. In this case, the frequency domain data needs to be passive so that the time domain response of the whole system can be guaranteed stable.

In the case when macromodeling is applied to handle the tabulated frequency domain data, enforcing the passivity of the model is a big issue. The time and effort spent in the passivity enforcement depends on the level of violation. Violation of the macromodel, in turn, is greatly influenced by the passivity violation of the original data. By correcting the passivity violation before the approximation, a lower level of passivity violation of the macromodel can be expected. Therefore, it is necessary to enforce passivity of the original data before doing an inverse Fourier transform or before approximating the data by macromodel.

### 6.3.1 Passivity check

The passivity criterion for the original frequency domain data is the same as that of the macromodel. That is, the impedance and admittance matrix should be positive real and the scattering matrix should be bounded real at any frequency.

For the transfer matrix $H(j\omega)$ to be positive real, the corresponding Hermitian matrix $G(j\omega)$, defined in the equation below, must be nonnegative definite for any frequency $\omega$ [60], i.e.,

$$G(j\omega) = \frac{1}{2}(H(j\omega) + H^H(j\omega)) \geq 0$$

where $H^H(j\omega)$ is the conjugate transpose of $H(j\omega)$. In order to meet the criterion described in the above equation, all eigenvalues of $G(j\omega)$ must be nonnegative at any frequency

$$\lambda(G(j\omega)) \geq 0$$

For scattering matrix, bounded real means that [60], [61]

$$I - H^H(j\omega)H(j\omega) \geq 0$$

at any frequency. The above requirement is equivalent to

$$\max \sigma(H(j\omega)) \leq 1 \tag{6.1}$$

which means that the maximum singular value of $H(j\omega)$ must be bounded by one at any frequency.

Scattering parameters are used as an example to illustrate the passivity restoration algorithm. Given scattering parameters, passivity check is first implemented to determine whether there are any passivity violations. The criterion described in Equation (6.1) is applied. The two plots below show the maximum singular value of the scattering

matrices versus frequency for two different cases. The horizontal axis is the frequency, and the vertical axis shows the maximum singular value of the scattering matrix.

Figure 6.2(a) shows the case where there is no passivity violation. The maximum singular value is less than one at all frequencies. However, Figure 6.2(b) shows singular values greater than one at some frequency points. Therefore, passivity violation exists and the data need to be corrected before applying the approximation or inverse fast Fourier transform (IFFT).

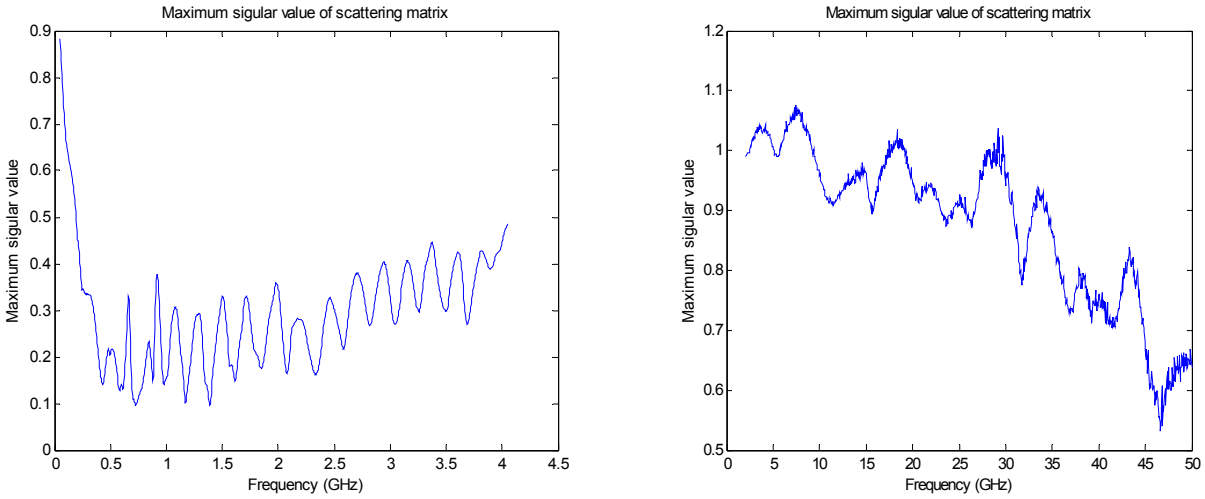


(a) (b)

Figure 6.2 (a) Data without passivity violation. (b) Passivity violated data.

### 6.3.2 Passivity enforcement

For cases where there is passivity violation, passivity enforcement must be applied to correct the raw data. In this work, the maximum singular value versus frequency plot, like the plots in Figure 6.2, is studied for passivity violations. For Figure 6.2(b), at frequencies where the maximum singular value is greater than one, the first-order perturbation is applied to the scattering matrix to restore the passivity of the system [60], [62].

**Lemma 6.1:** If a matrix is $Q$ is perturbed by an amount $\Delta Q$, then the resulting change in its eigenvalue ($\Delta\lambda$) is given by [62]

$$\Delta\lambda = \frac{u^T \Delta Q v}{u^T v}$$

where $u$ and $v$ are the left and right eigenvectors of $Q$, respectively.

For the scattering parameter case, passivity violation occurs when the eigenvalues of matrix $I - H^H H$ are less than zero, which means the eigenvalues of $H^H H$ are greater than one. Assume the eigenvalue of $I - H^H H$ is $\Delta\lambda < 0$ at some frequencies, the goal is to perturb the matrix $H$ by an amount $\Delta H$, so that the eigenvalue of matrix $I - (H + \Delta H)^H (H + \Delta H)$ is greater than or equal to zero [60]. In order to minimize the perturbation, the eigenvalue associated with the perturbed matrix is forced to zero. Therefore, by ignoring the second order term, we will have

$$\Delta\lambda = \frac{u^T (H^H \Delta H + \Delta H^H H) v}{u^T v}$$

where $u$ and $v$ are the left and right eigenvectors of $H^H H$, respectively.

The perturbation matrix $\Delta H$ can be obtained by solving the matrix equation below:

$$Wx = y \tag{6.2}$$

where $x$ is a column vector containing the elements of the perturbation matrix $\Delta H$, $y$ is the product of $\Delta\lambda$ and $u^t v$, and $W$ is a matrix consisting elements of $u$, $v$ and $H$. The derivation of matrix $W$ can be found below.

Define the perturbation matrix $\Delta H$ as

$$\Delta H = \begin{bmatrix} x_{11} & \cdots & x_{1n} \\ & \vdots & \\ x_{n1} & \vdots & x_{nn} \end{bmatrix}$$

and vector $x$ is defined as $x = [x_{11} \quad \cdots \quad x_{1n} \quad \cdots \quad x_{n1} \quad \cdots \quad x_{nn}]^T$. Matrix $W$ is composed of the scattering parameters of the system

$$H = \begin{bmatrix} s_{11} & \cdots & s_{1n} \\ & \vdots & \\ s_{n1} & \vdots & s_{nn} \end{bmatrix}$$

For $u^T(H^H \Delta H + \Delta H^H H)v$, the first term $u^T H^H \Delta H v$ can be expressed as the sum of the all the following terms

$$\begin{matrix} v_1 u_1 (s_{11}^* x_{11} + \cdots + s_{n1}^* x_{n1}) & \cdots & v_1 u_n (s_{11}^* x_{1n} + \cdots + s_{n1}^* x_{nn}) \\ v_n u_1 (s_{1n}^* x_{11} + \cdots + s_{nn}^* x_{n1}) & & v_n u_n (s_{1n}^* x_{1n} + \cdots + s_{nn}^* x_{nn}) \end{matrix} \tag{6.3}$$

The second term $u^T \Delta H^H H v$ can be expressed as the sum of the all the following terms

$$\begin{matrix} v_1 u_1 (x_{11}^* s_{11} + \cdots + x_{n1}^* s_{n1}) & \cdots & v_1 u_n (x_{11}^* s_{1n} + \cdots + x_{n1}^* s_{nn}) \\ & \vdots & \\ v_n u_1 (x_{1n}^* s_{11} + \cdots + x_{nn}^* s_{n1}) & & v_n u_n (x_{1n}^* s_{1n} + \cdots + x_{nn}^* s_{nn}) \end{matrix} \tag{6.4}$$

Separate the unknown variables from Equation (6.3), we will have

$$u^T H^H \Delta H v = Ax$$

where $A$ is a row vector and the element in $A$ corresponding to $x_{pq}$ is defined as $A_{pq} = u_q \sum_{i=1}^{n} v_i s_{pi}^*$. Similarly, Equation (6.4) can be written as

$$u^T \Delta H^H H v = Bx^*$$

and the elements in $B$ corresponding to $x_{pq}$ is defined as $B_{pq} = v_q \sum_{i=1}^{n} u_i s_{pi}^*$. Therefore, we have

$$Ax + Bx^* = \sum_{p=1}^{n} \sum_{q=1}^{n} (A_{pq} x_{pq} + B_{pq} x_{pq}^*) = y \tag{6.5}$$

Since the unknown variables contain both $x$ and its complex conjugate $x^*$, it is much more convenient to solve the real and imaginary parts of the unknowns separately. Let $x_{pq} = a_{pq} + jb_{pq}$. Equation (6.5) can be expressed as

$$\sum_{p=1}^{n}\sum_{q=1}^{n}[(A_{pq} + B_{pq})a_{pq} + j(A_{pq} - B_{pq})b_{pq}] = y \tag{6.6}$$

Let $E_{pq} = A_{pq} + B_{pq}$ and $F_{pq} = j(A_{pq} - B_{pq})$. We will have

$$\bar{W}\bar{x} = y \tag{6.7}$$

where $\bar{x} = [a_{11} \cdots a_{1n} \cdots a_{n1} \cdots a_{nn} \cdots b_{11} \cdots b_{1n} \cdots b_{n1} \cdots b_{nn}]^T$ and $\bar{W} = [E_{11} \cdots E_{1n} \cdots E_{n1} \cdots E_{nn} \cdots F_{11} \cdots F_{1n} \cdots F_{n1} \cdots F_{nn}]^T$.

Equation (6.7) is solved subject to the constraint of minimizing the norm of the perturbation matrix $\Delta H$.

## 6.4 Numerical Verification

This example shows the effect of the noise filtering to the macromodeling. As described in Section 6.2, the accuracy of the approximation can be improved by filtering out the noise from the measurement data.

For the data shown in Figure 6.1, approximation is done on both the original data and the noise filtered data. Below are some simulation results using the Chebyshev of the first kind for both cases. The same order of 65 is applied.

Figure 6.3(a) and (b) show the magnitude and phase of the original data and those from the approximation. The solid curve shows the original data, the dot-dashed curve is the approximation based on the original noisy data, and the dashed curve is the

approximation based on the noise filtered data. It is obvious that the dashed curve gives better approximation than the blue one for both magnitude and phase.

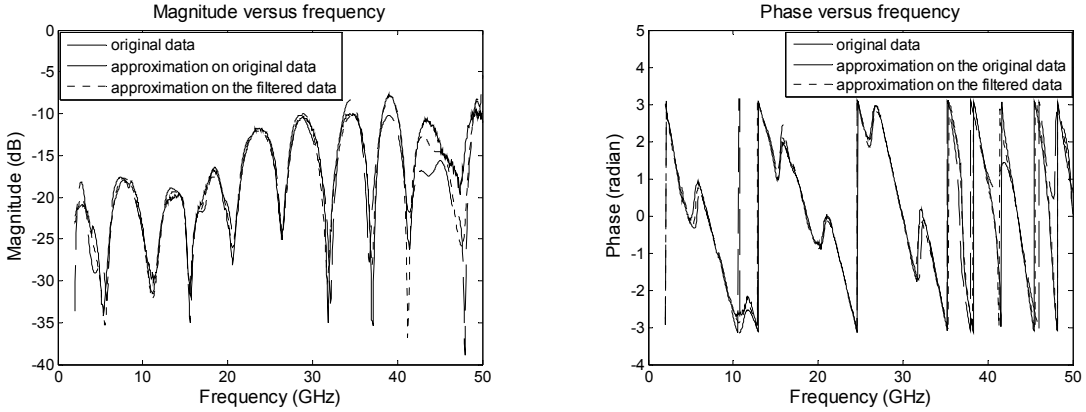


(a) Magnitude (b) Phase

Figure 6.3 Magnitude and phase of data.

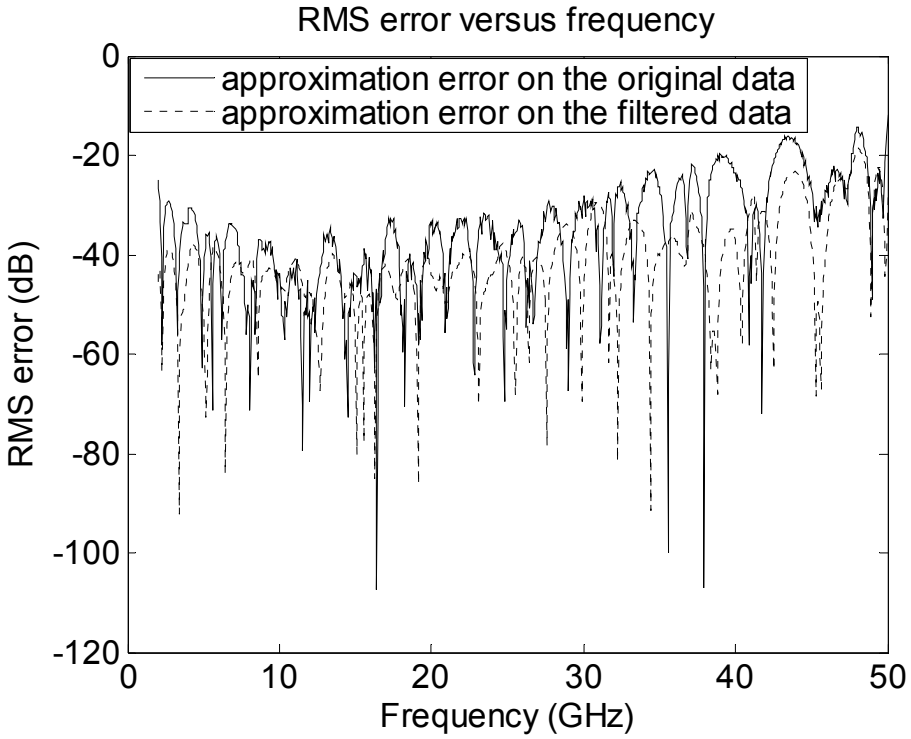


Figure 6.4 Root Mean Square error of the approximation.

Figure 6.4 shows the root mean square error of the approximation. The solid curve shows the RMS error of the approximation based on the original data and the dashed curve shows the RMS error of the approximation based on the data after noise filtering.

The result shows consistency with those in Figure 6.3. With the same approximation order, the approximation on the data with noise filtered gives more accuracy.

The numerical example below shows the effect of passivity enforcement for the data.

The data comes from a microstrip board. A total of 801 sampling points are given from 2 GHz to 50 GHz. The maximum singular value versus frequency of the data is shown in Figure 6.2(b), which has passivity violation at certain frequency points. Figure 6.5 shows the passivity restoration for parameters $S_{11}$ and $S_{12}$ using the first order perturbation described in Section 6.3. Both the original and passivity restored magnitude and phase are plotted.

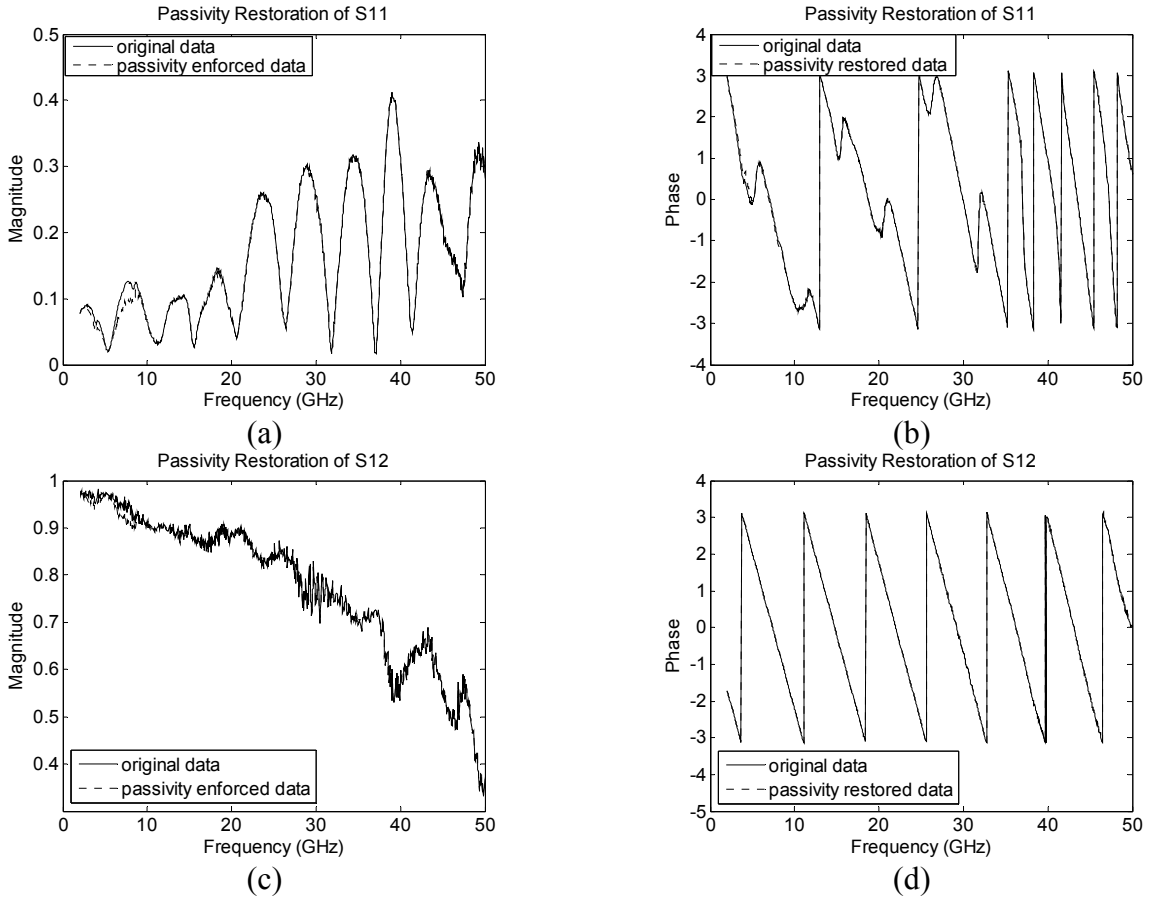


Figure 6.5 Passivity enforcement of the input data.

Figure 6.5(a) and (b) show the magnitude and phase of $S_{11}$ respectively, while (c) and (d) show the magnitude and phase of $S_{12}$. In all plots, the solid curve shows the original data and the dashed curve shows the passivity restored data. We can see from the plots that the data is modified at those frequencies where passivity is violated.

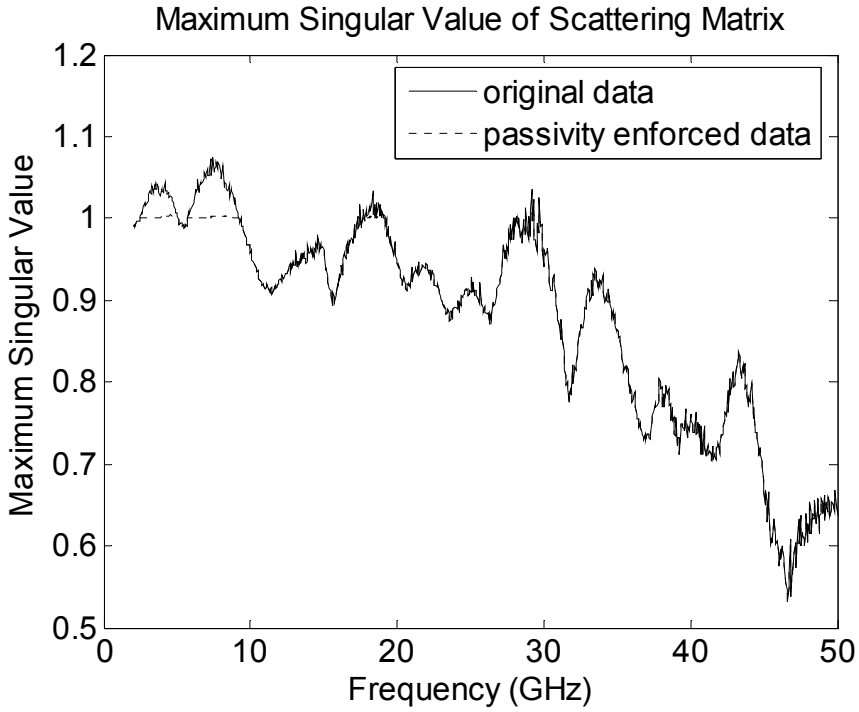


Figure 6.6. Maximum singular value of scatting matrix before and after passivity enforcement.

Figure 6.6 compares the maximum singular value of the original data and that of passivity restored data. The solid curve is the maximum singular value of the original data, while the dashed curve is the maximum singular value of the data with passivity enforced. From the comparison in Figure 6.6, it is clear that the first order perturbation algorithm described in this chapter successfully enforces the passivity of the data.

# 7 DELAY EXTRACTION

## 7.1 Introduction

An arbitrary system without a delay (or frequency-domain phase shift) can be approximated by a rational function with a finite number of poles and zeros. However, as the operating frequency of IC chips increases, time-domain delay becomes a significant characteristic of high-speed systems. Traditional rational function models encounter inherent difficulties in modeling systems that present considerable delays. The reason is because the time-domain delay takes the form of complex exponential shift, usually represented by $e^{-j\omega T_d}$, in the frequency domain. The exponential term, if represented by rational function, will need an infinite number of poles and therefore cannot be exactly modeled by any rational function with finite order. Hence, when the rational function is used to model a system with embedded delay, a much higher order is often necessary to maintain the modeling accuracy within the frequency band of interest.

The drawback of approximating systems with delay using only rational functions lies in several aspects. First, the high-order model increases the computational cost of both the model generation procedure and the successive simulations where the resultant model is used. Second, although the high-order model can maintain the accuracy within a certain frequency band, it might result in error outside the particular frequency range since the rational function does not capture the physical delay correctly. Therefore, it would be difficult to obtain a single rational function for a broad frequency band. Alternatively, the model order must increase as the frequency range becomes higher.

To reduce the order of approximation and sometimes guarantee causality, it is essential to first extract the delay of the system. The approach of combining the rational function and complex exponential shift term to model systems with delay has been investigated in several papers such as [63].

In this chapter, a new approach is presented to model a general network system by the product of a minimum phase rational function, an all-pass rational function and an exponential delay term. Hence we call it the MAD model. As will be discussed in the rest part of this chapter, this model will successfully describe most of the systems.

Compared to the traditional rational function approach, the MAD model has the following merits:

1. The physical time-domain delay can be explicitly extracted.
2. Since the delay is extracted, the remaining part of the system can be modeled accurately with a relatively low-order rational function.
3. A unified model can be obtained for a broad frequency range.

The rest part of this chapter is organized as follows. After an overview of the MAD model, the general procedure to obtain the proposed model is presented sequentially in the order of each step being performed, including minimum phase extraction, delay extraction, and model construction. Finally, the advantages of the MAD model are demonstrated by numerical examples.

## 7.2 MAD Model

In this section, it is proposed that a general $N$-port network can be modeled in terms of a minimum phase system, an all-pass system, and a delay term.

Suppose the system is an *N*-port network, of which $H(s)$ is the *S*-parameter matrix. We propose that each element of the $N \times N$ matrix $H(s)$ be characterized in the form of a rational function and a complex phase shift term as written below,

$$H_{ij}(s) = N_{ij}(s)e^{-s\tau_{ij}} \qquad i, j = 1, 2, \ldots, N \tag{7.1}$$

where $N_{ij}(s)$ is a rational function of $s$, which approximates the system function without delay between port $i$ and $j$. The term $\tau_{ij}$ is a nonnegative real number, which represents the delay between port $i$ and $j$.

The difference between this model and the traditional rational function model lies in the delay term. For high-speed complex structures, delay is a very important factor and it cannot be exactly modeled with a rational function. If merely a rational function is used to approximate the system with delay, the order of the resultant transfer function has to be unnecessarily high to maintain the same accuracy. Furthermore, even if the physical system does not change, the model order still needs to keep increasing if the frequency range of interest increases.

The proposed model overcomes the above problem by extracting the delay term explicitly. As a result, a relatively low-order rational function, together with the delay term, can provide an accurate model. Therefore, both model accuracy and efficiency are improved.

Any stable and causal rational transfer function can be decomposed into a minimum phase system and an all-pass system [38]. Therefore, (7.1) can be written as

$$H_{ij}(s) = M_{ij}(s)P_{ij}(s)e^{-s\tau_{ij}} \tag{7.2}$$

where $M_{ij}(s)P_{ij}(s) = N_{ij}(s)$, $M_{ij}(s)$ is a minimum phase system, and $P_{ij}(s)$ is an all-pass system.

The minimum phase system is not only causal and stable, but also has causal and stable inverse. That is, all the poles and zeros of the minimum phase system are in the left half of the complex plane.

The all-pass system has constant magnitude over the whole frequency range. The poles and zeros of the all pass system are symmetric about the imaginary axis in the complex plane.

For any stable and causal rational function $H_{ij}(s)$, the poles are all in the left half of the complex plane due to the stability constraints. However, the zeros can be anywhere in the complex plane except that they should be symmetric about the real axis so that real coefficients of the rational function are guaranteed. For a rational function with zeros in the right half plane, the zeros can be reflected to the left half plane. Therefore, the original system is decomposed into two systems: a minimum phase system with poles of the original system and the reflected zeros, and an all pass system with poles at where the reflected zeros are and zeros in the original right half plane.

This fact is best illustrated in Figure 7.1. The poles of the system are represented by crosses, and zeros are represented by circles. Any causal and stable system $N_{ij}(s)$ is a multiplication of the minimum phase system $M_{ij}(s)$ and the all pass system $P_{ij}(s)$. The right half plane zeros of $N_{ij}(s)$ are reflected to those circled zeros of $M_{ij}(s)$. The circled

zeros of $M_{ij}(s)$ and poles of $P_{ij}(s)$ cancel each other by multiplication. Thus, the rational function $H_{ij}(s)$ is successfully decomposed.

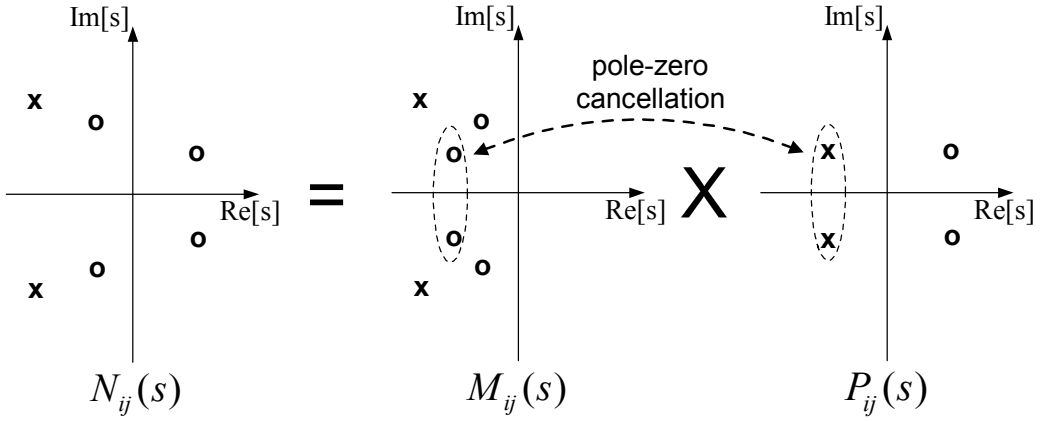


Figure 7.1 A stable and causal rational system can always be decomposed into a minimum phase system and an all-pass system.

## 7.3 Minimum Phase Extraction

From Equation (7.2), we have

$$|H_{ij}(s)| = |M_{ij}(s)||P_{ij}(s)||e^{-s\tau_{ij}}| \tag{7.3}$$

Let $s = j\omega$, and since $|P_{ij}(j\omega)| = |e^{-j\omega\tau_{ij}}| = 1$, we will have

$$|H_{ij}(j\omega)| = |M_{ij}(j\omega)| \tag{7.4}$$

For simpler expression, the functions in Equation (7.4) will be written in terms of $\omega$ instead of $j\omega$ in the discussions below. The other expressions used below are $\arg[\ ]$, which represents the continuous phase, and $grd[\ ]$, which is the corresponding group delay, a negative gradient of the continuous phase.

The phase of a minimum phase system can be completely determined by its magnitude via the Hilbert transform [64], [65]:

$$\arg[M_{ij}(\omega)] = \frac{2\omega}{\pi}\int_0^{\infty}\frac{U(\xi)-U(\omega)}{(\xi+\omega)(\xi-\omega)}d\xi \tag{7.5}$$

where $U(\omega) = \ln|M_{ij}(\omega)| = \ln|H_{ij}(\omega)|$. Therefore, from the measured or simulated data $H_{ij}(\omega)$, the angle of the minimum phase part, $\arg[M_{ij}(\omega)]$, can be obtained numerically from Equation (7.5). After the magnitude and phase of $M_{ij}(\omega)$ are determined in terms of the discrete data set, the orthogonal polynomial method can be used to construct the transfer function representation for $M_{ij}(\omega)$. According to the property of the minimum phase system that the energy in a minimum phase transient response occurs earlier in time than for a nonminimum phase waveform with the same spectral magnitude [38], $M_{ij}(\omega)$ should contain the least delay among all rational functions with the same spectral magnitude. Therefore, $M_{ij}(\omega)$ can be accurately constructed with a relatively low-order.

## 7.4 Delay Extraction

Once the minimum phase part of the system is separated, the rest of the system can be obtained from Equation (7.2). Define

$$X_{ij}(\omega) = \frac{H_{ij}(\omega)}{M_{ij}(\omega)} = e^{-j\omega\tau_{ij}} \times P_{ij}(\omega) \tag{7.6}$$

we have the following phase relationship,

$$-\omega\tau_{ij} = \arg[X_{ij}(\omega)] - \arg[P_{ij}(\omega)] = \arg[H_{ij}(\omega)] - \arg[M_{ij}(\omega)] - \arg[P_{ij}(\omega)] \tag{7.7}$$

Taking the derivative of (7.7) with respect to $\omega$ and the negative gradient gives the group delay, which yields,

$$\tau_{ij} + grd\left[\arg[P_{ij}(\omega)]\right] = grd\left[\phi_{ij}(\omega)\right] \tag{7.8}$$

where $\phi_{ij}(\omega) = \arg\left[X_{ij}(\omega)\right] = \arg[H_{ij}(\omega)] - \arg[M_{ij}(\omega)]$. Obviously, $\phi_{ij}(\omega)$ can be obtained numerically from the angle of the original system and that of the minimum phase system. The phase of $H_{ij}(\omega)$ can be obtained directly from the given frequency response. The phase of the minimum phase system, $\arg\left[M_{ij}(\omega)\right]$, can be calculated from Equation (7.5) given the magnitude of the frequency response. Once we have $\phi_{ij}(\omega)$, we can calculate the summation of the system delay $\tau_{ij}$ and the negative phase gradient of the all pass system $P_{ij}(\omega)$ from Equation (7.8). By definition, $\tau_{ij}$ is a constant independent from the frequency $\omega$. To estimate $\tau_{ij}$, we need to analyze the characteristics of $grd\left[\arg[P_{ij}(\omega)]\right]$.

Since $P_{ij}(\omega)$ is an all-pass system, its poles and zeros exist in pairs located symmetrically with respect to the imaginary axis; that is, each pole corresponds to a zero located at its mirror point with respect to the imaginary axis and vice versa. Additionally, since $H_{ij}(\omega)$ is a physical system, both $M_{ij}(\omega)$ and $P_{ij}(\omega)$ are supposed to be rational functions with only real coefficients and hence their poles and zeros are symmetric with respect to the real axis. All the poles are located in the left half of the complex plane. Therefore, $P_{ij}(\omega)$ can be expressed in the following form

$$P_{ij}(\omega) = \prod_{k=1}^{N_p/2} \frac{j\omega - (a_k + jb_k)}{j\omega - (-a_k + jb_k)} \frac{j\omega - (a_k - jb_k)}{j\omega - (-a_k - jb_k)} \tag{7.9}$$

where $N_p$ is the number of poles or zeros of $P_{ij}(\omega)$, $a_k$'s and $b_k$'s are positive real numbers.

To simplify the discussion in this section, the symmetry of poles and zeros with respect to the real axis is not considered, so we write Equation (7.9) in a more general form as:

$$P_{ij}(\omega) = \prod_{k=1}^{N_p} \frac{j\omega - (a_k + jc_k)}{j\omega - (-a_k + jc_k)} \tag{7.10}$$

where $c_k$ 's are nonzero real numbers. Obviously,

$$\arg\left[ P_{ij}(\omega) \right] = \sum_{k=1}^{N_p} \alpha_k \tag{7.11}$$

where

$$\alpha_k = \arg\left[ \frac{j\omega - (a_k + jc_k)}{j\omega - (-a_k + jc_k)} \right] = \arg[j\omega - (a_k + jc_k)] - \arg[j\omega - (-a_k + jc_k)] \tag{7.12}$$

Equation (7.11) illustrates that the phase of $P_{ij}(\omega)$ is the sum of phase contributions from each pole-zero pair.

Next we discuss the phase contribution from a single pole-zero pair.

As shown in Figure 7.2, $\alpha_k = \alpha_{k1}$ when $s = j\omega_1$ and $\alpha_k = \alpha_{k2}$ when $s = j\omega_2$. As $\omega$ varies from $-\infty$ to $jc_k$, $\alpha_k$ decreases monotonically from 0 to $-\pi$. As $\omega$ varies from $jc_k$ to $\infty$, $\alpha_k$ decreases monotonically from $-\pi$ to $-2\pi$. Here we choose the range of $\alpha_k$ such that $\alpha_k$ is a continuous function of $\omega$ for $\omega \in (-\infty, \infty)$.

Under this condition, $\alpha_k$ is monotonically decreasing for $\omega \in (-\infty, \infty)$. Therefore,

$$grd[\alpha_k] \geq 0, \quad \text{for } \omega \in (-\infty, \infty) \tag{7.13}$$

Assuming $c_k$ is finite, it is straightforward to prove from Equation (7.12) that

$$\lim_{|\omega| \to \infty} grd[\alpha_k] = 0 \tag{7.14}$$

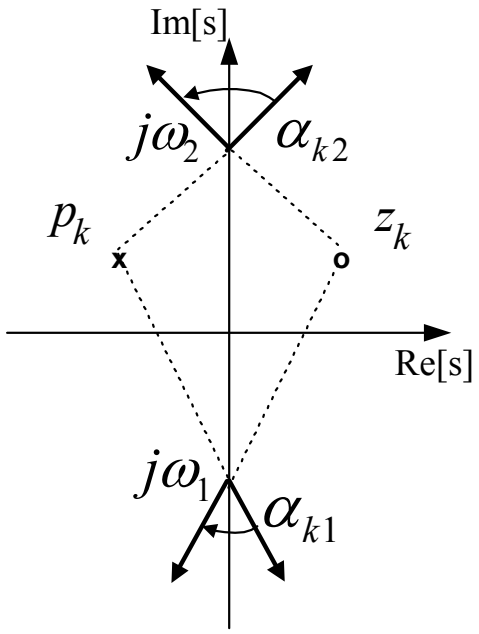


Figure 7.2 Phase contribution of a pole-zero pair of the all-pass system.

Hence, from Equation (7.11), we have

$$grd[\arg[P_{ij}(\omega)]] \geq 0, \quad \text{for } \omega \in (-\infty, \infty) \tag{7.15}$$

and

$$\lim_{|\omega| \to \infty} grd[\arg[P_{ij}(\omega)]] = 0 \tag{7.16}$$

Considering (7.8) and (7.15), and the fact that $\tau_{ij}$ is a constant independent from $\omega$, we propose a simple approach to estimating $\tau_{ij}$ as follows.

$$\tau_{ij} = \min_{\omega \in [\omega_{\min}, \omega_{\max}]} grd[\phi_{ij}(\omega)] \tag{7.17}$$

where $\omega_{\min}$ and $\omega_{\max}$ are respectively the lower and upper limits of the frequency range, in which the data for $grd[\phi_{ij}(\omega)]$ is available. Equation (7.17) is accurate if $[\omega_{\min}, \omega_{\max}]$ is broad enough to satisfy

$$\min_{\omega\in[\omega_{\min},\omega_{\max}]} grd[\arg[P_{ij}(\omega)]] = 0 \tag{7.18}$$

Equation (7.18) might not be satisfied, that is,

$$\min_{\omega\in[\omega_{\min},\omega_{\max}]} grd[\arg[P_{ij}(\omega)]] = \delta > 0 \tag{7.19}$$

In this case, the estimate of $\tau_{ij}$ using Equation (7.17) is not the actual delay of the system as it would be if $grd[\phi_{ij}(\omega)]$ were available in a broader frequency range. However, this does not compromise the accuracy of the entire model, because Equation (7.19) means nothing but that the effect of the all-pass system is partially taken care of by the delay term. Although we call $e^{-j\omega\tau_{ij}}$ as the delay term because it does characterize the physical delay, more generally speaking, it is just one term that captures the system characteristics in addition to the rational function.

The algorithm of capturing the delay of the system and construct the MAD model is given in pseudocode in Algorithm 7.1.

**Algorithm 7.1:** Delay extraction

1. *Read the frequency domain data and find the magnitude of the frequency response.*
2. *Calculate the phase of the minimum phase system,* $\arg[M_{ij}(\omega)]$*, using Equation (7.5).* $U(\omega) = \ln|M_{ij}(\omega)|$. *The magnitude of the minimum phase system is the same as that of the original system.*
3. *Remove the response of the minimum phase system from the original frequency response as per Equation (7.6). The resulted system is defined as* $X_{ij}(\omega)$.
4. *Group delay of* $X_{ij}(\omega)$ *from step 3 is the summation of the delay term and the negative phase gradient of the all pass system.*
5. *Separate the delay from step 4. The delay is found within the valid frequency range.*
6. *Approximate the system without delay using the orthogonal polynomial approximation described in Chapter 4.*

## 7.5 Numerical Results

### 7.5.1 Numerical validation

To validate the proposed method, we generate the frequency domain data from a known system, which is a rational function with a certain amount of delay inserted. Here, we consider two cases, (1) the rational function is a minimum phase system, and (2) it is a nonminimum phase system. Most realistic systems are in the category (2). Then the delay is extracted by the proposed method and compared with the original inserted amount, which is 0.3 ns for both cases.

The group delay after minimum phase extraction is illustrated in Figure 7.3 for both cases.

Ideally, the group delay in Figure 7.3(a) should be constant over the whole frequency range, since it only contains the contribution from the delay term. It is actually not constant due to numerical error in minimum phase extraction process. The original data is only available in a finite frequency range. However, the Hilbert transform described in Equation (7.5), which relates the magnitude and phase of the minimum phase subsystem, is calculated over the frequency from zero to infinity. Hence, the minimum phase extraction becomes inaccurate when frequency approaches the band limit of the original data. The minimum phase system should ideally have the same magnitude as the original data. Hence, we can determine the valid frequency range for delay extraction by comparing the extracted minimum phase magnitude with the original magnitude. In Figure 7.3(b), the group delay contains both the delay term and the all-pass term.

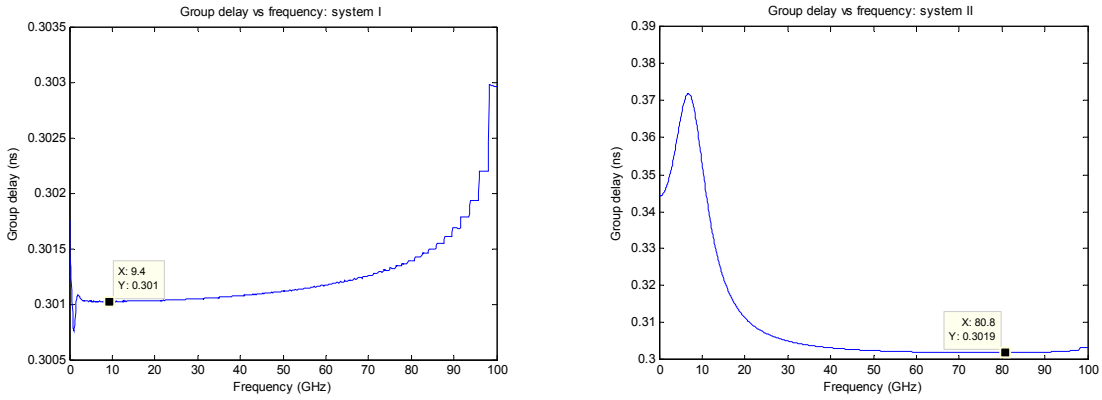


(a) (b)

Figure 7.3 Group delay after minimum phase extraction. (a) Group delay for case 1 and (b) group delay for case 2.

From Figure 7.3(a), the delay is found to be 0.301 ns, which gives an error of 0.33% percent. From Figure 7.3(b), the peak in the low frequency reflects the group delay of the all pass term. Since the all pass term has positive group delay, the delay in the system should be the minimum group delay in the valid frequency range. The delay in this case is found to be 0.3019 ns, which gives an error of 0.63%. In both cases, we will have the percentage error under 1%, which demonstrates the accuracy of the proposed method.

### 7.5.2 Coupled via delay extraction

Figure 7.4 shows the delay extraction for four-port data of coupled via. The data is calculated from CST field solver. The delay is extracted for different ports. Below are plots showing the delay for data: $S_{11}$, $S_{12}$, $S_{13}$, $S_{14}$, $S_{22}$, $S_{23}$, $S_{24}$, $S_{33}$, $S_{34}$ and $S_{44}$.

From the group delay versus frequency plots, it is obvious that the delay in each port can be effectively extracted. The vertical value of the point in each plot shows the delay between the corresponding ports.

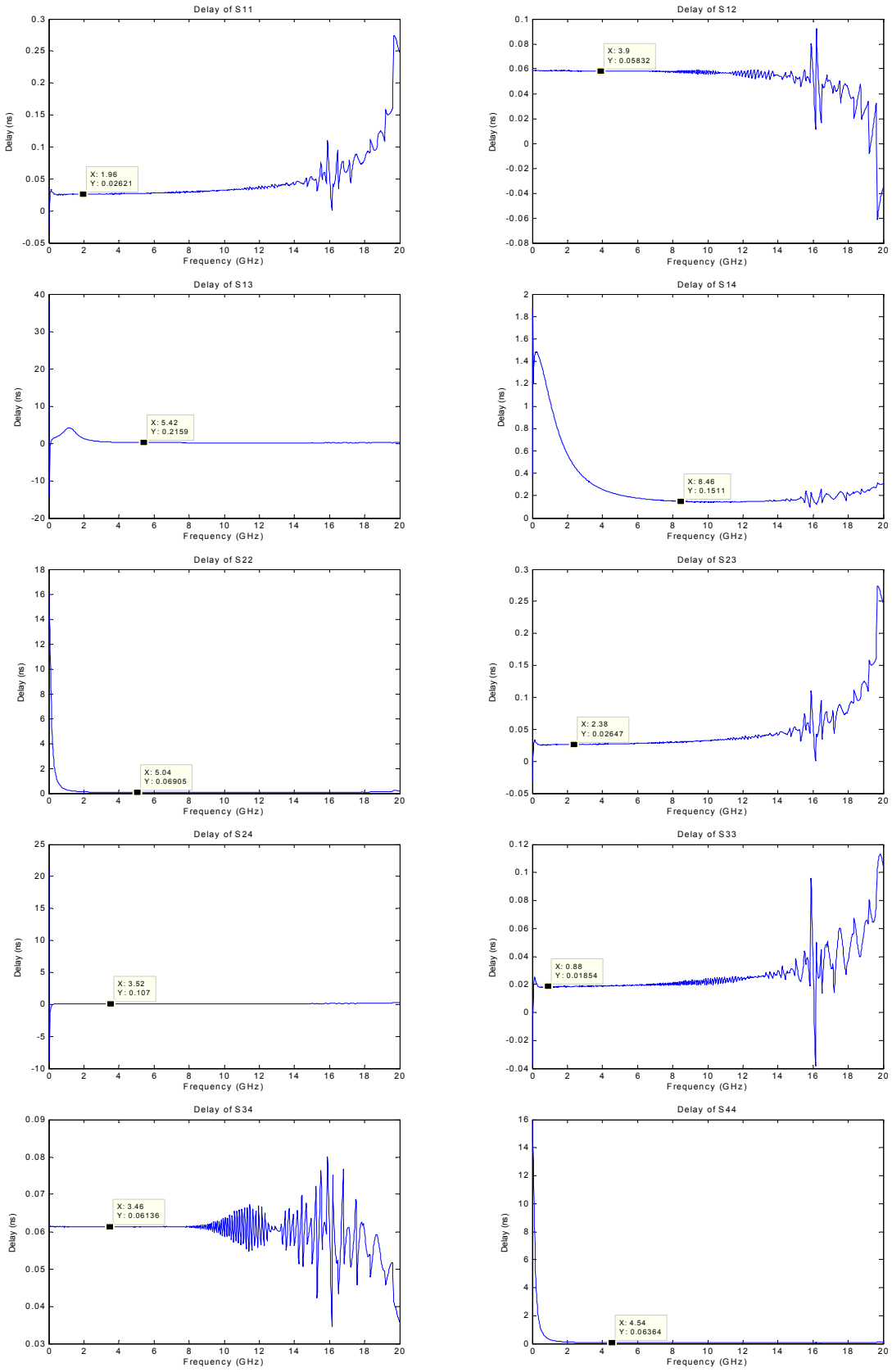


Figure 7.4 Delay extraction for coupled via.

### 7.5.3 A transmission line with discontinuities

Figure 7.5 shows a transmission line with discontinuities. The length of the line is 7 in. The scattering parameter is measured from 0.3 MHz to 6 GHz. A total of 1601 frequency samplings are provided at a spacing of 3.75 MHz.

Figure 7.5 Transmission line with discontinuities.

Since the delay is different between different ports, the delay extraction is implemented on all four scattering parameters. Figure 7.6 shows the group delay after the minimum phase subsystem has been removed from the frequency response.

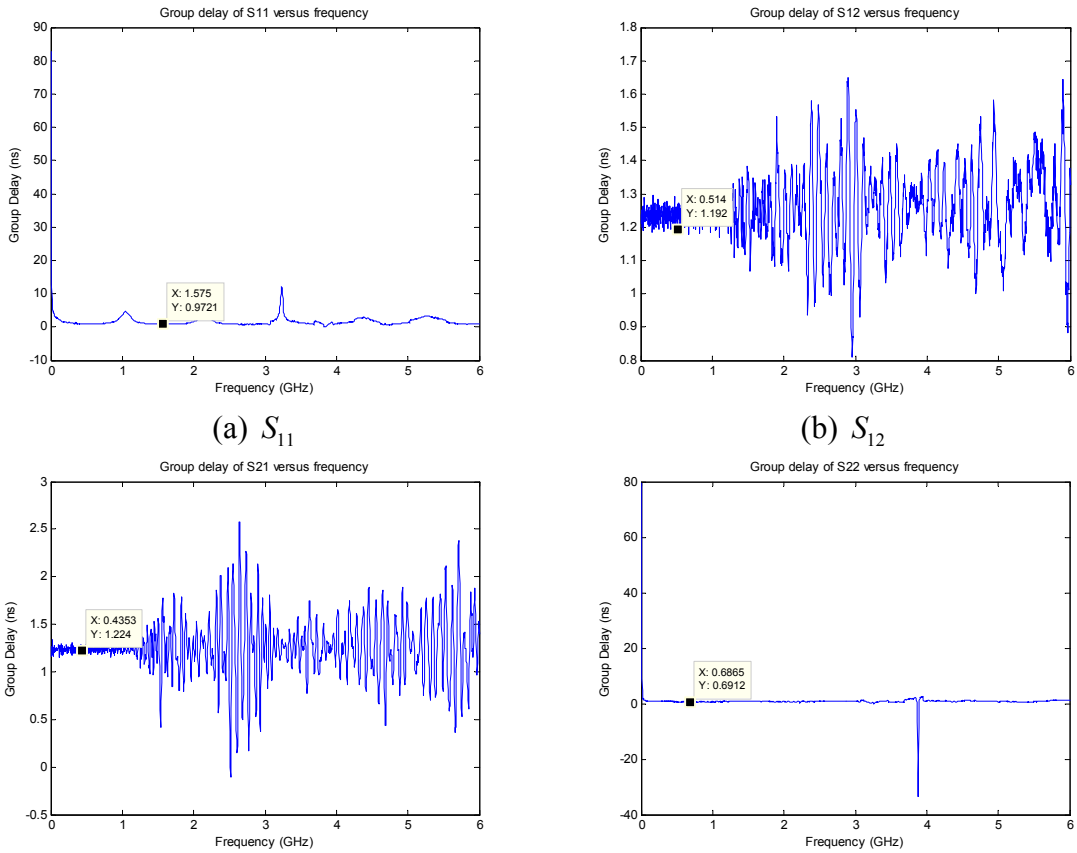


(a) $S_{11}$ (b) $S_{12}$

(c) $S_{21}$ (d) $S_{22}$

Figure 7.6 Group delay after minimum phase extraction.

To eliminate the effect of numerical noise amplified by the gradient operation, moving average filtering is performed after taking the gradient. The amount of delay is determined by finding the minimum group delay within the valid frequency range. The delays extracted are approximately 0.9721 ns for $S_{11}$, 1.192 ns for $S_{12}$, 1.224 ns for $S_{21}$, and 0.6912 ns for $S_{22}$.

Once the delay is extracted from the frequency response of the system, we only need to approximate the rest of the system using the approach discussed in Chapter 4.

From Figure 7.6, it is apparent that, with the minimum phase subsystem removed, the phase gradient is not flat over the whole frequency. This shows the presence of the all-pass term in this case. The results below will distinguish the advantage of the MAD method from other methods.

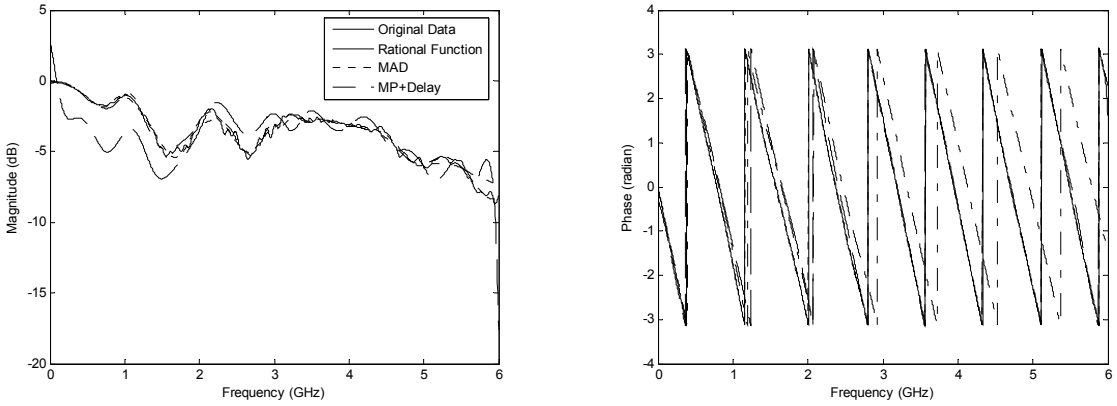


(a) Magnitude (b) Phase

Figure 7.7 The $S_{12}$ parameter obtained respectively by the traditional rational function method, the MAD method, and the minimum-phase-plus-delay method.

The system is modeled respectively by traditional rational function method, the MAD method and the minimum-phase-plus-delay method. Figure 7.7 shows the magnitudes and phases for $S_{12}$ obtained respectively by the three methods, which all use

the same order of 40. It is clear that the MAD method provides much better accuracy than the other two methods. The minimum-phase-plus-delay model provides slightly worse accuracy than the MAD method in magnitude but significantly larger error in phase. The MAD method shows excellent accuracy in both magnitude and phase.

## 7.6 Conclusion

A new black box modeling approach called MAD method is presented by decomposing a realistic system into a minimum phase system, an all-pass system and a delay term. This method correctly captures the major physical characteristics of high-speed networks. Hence, it significantly improves the modeling accuracy and efficiency compared to earlier methods.

# 8 CONCLUSIONS AND FUTURE WORK

## 8.1 Conclusions

In this work, the black box modeling of passive systems characterized by simulated or measured frequency domain data is discussed. Rational function approximation using orthogonal polynomials was shown to be an efficient method. Based on the results obtained, the following conclusions can be drawn.

- Rational function approximation using orthogonal polynomials is shown to be an efficient and accurate method for black box modeling. The properties of a physical linear system are incorporated in the approximation and thus stability and causality are inherently ensured. Passivity is enforced by a systematic approach based on perturbation theory.
- The necessity and effect of data preprocessing including noise filtering and passivity check are demonstrated. Noise filtering of the input data reduces the required order of the resultant macromodel and hence improves the modeling efficiency. The passivity enforcement to the input data releases the difficulty of the later passivity enforcement to the macromodel.
- A new method called MAD method is presented to model a system by a minimum phase term, an all pass term, and a delay term. A systematic procedure is developed to implement this method. As demonstrated by numerical results, this new method improves both the accuracy and efficiency of the modeling process. The fundamental reason is that the MAD model precise captured the physical characteristics of the system.

## 8.2 Future Work

Possible future work includes research on more efficient model order estimation and passivity enforcement methods for the macromodel. The current model order estimation involves finding matrix eigenvalues, which is computationally expensive, especially for high order systems. The current passivity enforcement method is limited by the nature of perturbation theory and therefore requires the passivity violation be relatively small. A better approach should be incorporated into the initial construction of the macromodel.

# REFERENCES


[1] E. Ruehli, "Equivalent circuit models for three dimensional multiconductor systems," *IEEE Trans. Microwave Theory Tech.,* vol. 22*,* pp. 216-221, March 1974.

[2] E. Chiprout and M. S. Nakhla, *Asymptotic Waveform Evaluation and Moment Matching of Interconnect Analysis.* Boston, MA: Kluwer, 1994.

[3] L. T. Pillage and R. A. Rohrer, "Asymptotic waveform evaluation for timing analysis," *IEEE Trans. Computer-Aided Design*, vol. 9, pp. 352-366, Apr. 1990.

[4] J. E. Bracken, V. Raghavan, and R. A. Rohrer, "Interconnect simulation with asymptotic waveform evaluation (AWE)," *IEEE Trans. Circuits Syst. I*, vol. 39, pp. 869-878, Nov. 1992.

[5] P. Feldmann and R. W. Freund, "Efficient linear circuit analysis by Pade approximation via Lanczos process," *IEEE Trans. Computer-Aided Design*, vol. 14, pp. 639-649, May 1995.

[6] G. A. Baker, Jr. and P. Graves-Morris, *Padé Approximation, Part I: Basic Theory.* Reading, MA: Addison-Wesley, 1981.

[7] E. Chiprout and M. S. Nakhla, "Analysis of interconnect networks using complex frequency hopping (CFH)," *IEEE Trans. Computer-Aided Design*, vol. 14, pp. 186-200, Feb 1995.

[8] M. Celik and A. C. Cangellaris, "Efficient transient simulation of lossy packaging interconnects using moment matching techniques," *IEEE Trans. Comp. Packag. Manufac. Technol. B,* vol. 19, pp. 64-73, Feb. 1996.

[9] E. J. Grimme, "Krylov projection methods for model reduction," Ph.D. dissertation, Univ. Illinois at Urbana–Champaign, 1997.

[10] C. Lanczos, "An iteration method for the solution of the eigenvalue problem of linear different and integral operations," *J. Res. Nat. Bur. Standards*, vol. 45, pp. 225-282, 1950.

[11] W. T. Beyene and J. E. Schutt-Aine, "Model order reduction techniques for circuit and interconnects simulation," University of Illinois at Urbana-Champaign, Electromagnetics Laboratory Scientific Report, No. 97-1, Feb. 1997.

[12] K. J. Kerns, I. L. Wemple, and A. T. Yang, "Stable and efficient reduction of substrate model networks using congruence transforms," in *Proc. ICCAD'95*, November 1995, pp. 207-214.

[13] L. M. Elfadel and D. D. Ling, "Block rational Arnoldi algorithm for multi-port passive model-order reduction of multi-port RLC networks," in *Proc. ICCAD'97,* Nov. 1997, pp. 66-71.

[14] D. L. Boley, "Krylov space methods on state-space control models," *Circuits Syst. Signal Processing*, vol. 13, no. 6, pp. 733-758, 1994.

[15] S. H. Min and M. Swaminathan, "Efficient construction of two-port passive macromodels for resonant networks," in *Proceedings of IEEE 10th Topical Meeting on Electrical Performance of Electrical Packaging,* Oct. 2001, pp. 229-232.

[16] S. H. Min, "Automated construction of macromodels from frequency data for simulation of distributed interconnect networks," Ph.D. dissertation, Georgia Institute of Technology, Apr. 2004.

[17] K. L. Choi and M. Swaminathan, "Development of model libraries for embedded passives using network synthesis," *IEEE Trans. Analog Digital Signal Processing*, vol. 47, no. 4, pp. 249-260. April 2000.

[18] W. T. Beyene and J. E. Schutt-Aine, "Efficient transient simulation of high-speed interconnects characterized by sample data," *IEEE Trans. Comp. Packag. Manufac. Tech.*, vol. 21, pp. 105-114, Feb 1998.

[19] R. Gao, Y. S. Mekonnen, W. T. Beyene, and J. E. Schutt-Aine, "Black-box modeling by rational function approximation," in *Proceedings of IEEE Workshop on Signal Propagation in Interconnects*, SPI- 2004, pp. 203-210.

[20] F. J. Casa, J. Portilla, R. Quere, A. Mallet, and J. Francois, "Model-order reduction of linear and weakly nonlinear time-varying RF and microwave circuits," *IEEE Trans. Microwave Theory Techniques,* vol. 52, no. 9, pp. 2262-2273, Sept. 2004.

[21] Y. S. Mekonnen, W. T. Beyene, and J. E. Schutt-Aine, "Improved high-order approximation by combining rational interpolation with the vector fitting method," in *20th Annual Review of Progress in Applied Computational Electromagnetic*, Syracuse, NY, April 19-23, 2004, pp. 104-109.

[22] W. T. Beyene, "Improving time-domain measurements with a network analyzer using a robust rational interpolation technique," *IEEE Trans. Microwave Theory and Techniques*, vol. 49, no. 3, pp. 500-508, March 2001.

[23] D. Saraswat, R. Achar, and M. Nakhla, "A fast algorithm and practical considerations for passive macromodeling of measured/simulated data," *IEEE Trans. Advanced Packing,* vol. 27, no. 1 pp. 57-70, Feb. 2004.

[24] B. Gustavsen and A. Semlyen, "Enforcing passivity for admittance matrices approximated by rational functions," *IEEE Trans. Power Systems*, vol. 16, pp. 97-104, Feb. 2001.

[25] S. Grivet-Talocia, "Enforcing passivity of macromodels via spectral perturbation of the Hamiltonian matrices," in *Proceedings of IEEE Workshop on Signal Propagation in Interconnects*, May 2003, pp. 287-290.

[26] S. Grivet-Talocia, "Passivity enforcement via perturbation of Hamiltonian matrices," *IEEE Transaction on Circuits Syst.*, vol. 51, no. 9, pp. 1755-1769, Sep. 2004.

[27] A. Odabasioglu, M. Celik and L. T. Pileggi, "PRIMA: Passive reduced-order interconnect macromodeling algorithm," *IEEE Trans. Computer-Aided Design Integ. Circuits Syst.*, vol. 17, no.8, pp. 645-654, August 1998.

[28] D. Saraswat, R. Achar, and M. Nakhla, "Passive reduction algorithm for RLC interconnect circuits with embedded state-space systems (PRESS)," *IEEE Trans. Microwave Theory Techniques*, vol. 52, no. 9, pp. 2215-2226, Sep. 2004.

[29] C-W Ho, E. Ruehli and P. A. Brennan, "The modified nodal approach to network analysis," *IEEE Trans. Circuits Syst.,* CAS-25, pp. 504-509, June 1975.

[30] L.M Wedepohl and L. Jackson, "Modified nodal analysis: an essential addition to electrical circuit theory and analysis," *Engineering Science and Education Journal,* Vol. 11, Issue 3, pp. 84 – 92, June 2002 .

[31] Q. Yu, J.Wang and E. S. Kuh, "Passive multipoint moment matching model order reduction algorithm on multi-port distributed interconnect networks," *IEEE Trans. Circuits Syst.*, vol. 46, pp. 140-160, January 1999.

[32] J. R. Marti, "Accurate modeling of frequency-dependant transmission lines in electromagnetic transient simulations," *IEEE Trans. Power Apparatus Syst.,* vol. 101, no. 1, pp. 147-157, January, 1982.

[33] B. Gustavsen and A. Semlysen, "Rational approximation of frequency domain response by vector fitting," *IEEE Trans. Power Delivery*, vol. 14, no. 3, pp. 1052-1061, July, 1999.

[34] M. Celik, O. Ocali, and M. A. Tan, "Pole-zero computation in microwave circuits using multiport Padé approximation," *IEEE Trans. Circuits Syst., I,* vol. 42, pp.6-13, Jan. 1995.

[35] S. Sakata, "Partial realization of 2-D discrete linear system and 2-D Padé approximation and reduction of 2-D rational transfer function," *Proc. IEEE*, vol. 78, pp. 604-613, April 1990.

[36] A. Alkhairy, "Design of IIR filter with arbitrary magnitude," *IEEE Transactions on Circuits and Systems-11: Analog and Digital Signal Processing,* Vol. 42**.** No. 9, pp. 618-620, Sept. 1995

[37] R. Mohan, M. J. Choi, S. E. Mick, F. P. Hart, K. Chandrasekar, A. C. Cangellaris, P. D. Franzon, and M. B. Steer, "Causal reduced-order modeling of distributed structures in a transient circuit simulator," *IEEE Trans. Microwave Theory and Techniques,* vol. 52, no. 9, pp. 2207-2214, Sept. 2004.

[38] A. V. Oppenheim and R. W. Schafer, *Discrete-Time Signal Processing.* Upper Saddle River, NJ: Prentice Hall, 1999.

[39] V. Belevitch, *Classical Network Theory.* San Francisco, CA: Holden-Day, 1968.

[40] R. Achar and M. Nakhla, "Simulation of high-speed interconnects," *Proc. IEEE*, vol. 89, pp. 693-728, May 2001.

[41] E. Kuh and R. Rohrer, *Theory of Active Linear Networks*. San Francisco, CA: Holden-Day, 1967.

[42] L. Weinberg, *Network Analysis and Synthesis*. New York: McGraw-Hill, 1962.

[43] S. Grivet-Talocia, "Enforcing passivity of macromodels via spectral perturbation of Hamiltonian matrices, " in *7th IEEE Workshop on Signal Propagation on Interconnects (SPI)*, Siena, 2003, pp. 33-36.

[44] C. E. Baumgartner, "On the representation of coupled lossy transmission lines using transfer function," *Ninth Annual International Phoenix conference on Computers and Communications,* Scottsdale, AZ, March 21-23, 1990.

[45] D. L. Fletcher and C. N. Weygandt, "A digital method of transfer function calculation," *IEEE Trans. Circuit Theory,* vol. CT-18, pp. 185-187, January, 1971.

[46] R. S. Adve, T. K. Sarkar, S. M. Rao, E. K. Miller, and D. R. Pflug, "Application of the cauchy method for extrapolating/interpolating narrow-band system responses, " *IEEE Trans. Microwave Theory Techniques,* vol. 45, no. 5, pp. 2743-2760, May. 1997.

[47] R. Gao, Y. S. Mekonnen, W. T. Beyene, and J. E. Schutt-Aine, "Black-box modeling of passive systems by rational function approximation," *IEEE Trans. Advanced Packaging*, vol. 28, no. 2, pp. 209-215, May 2005.

[48] W. H. Press, S. A. Teukolsky, V. T. Vetterling, and B. P. Flannery, *Numerical Recipes in C++*. Cambridge, U. K: Cambridge Univ. Press, 2002, pp. 187-189.

[49] H. Akaike, "A new look at the statistical model identification," *IEEE Trans. Automatic Control,* vol. AC-19, pp. 716-723, 1974.

[50] Y. Barron, J. Rissanen and B. Yu, "The minimum description length principle in coding and modeling," *IEEE Trans. Information Theory,* vol. 44, pp. 2743-2760, Oct. 1998.

[51] S. Beheshti and M. A. Dahleh, "LTI systems, additive noise, and order estimation," in *Proc. 42nd IEEE Conference on Decision and Control*, vol. 6, Dec. 9-12, 2003, pp. 6491-6496.

[52] K. L. Choi, "Modeling and Simulation of Embedded Passives Using Rational Functions in Multi-layered Substrates," Ph.D. Thesis, Georgia Institute of Technology, August 1999.

[53] G. H. Golub and C. F. Van Loan, *Matrix Computation.* Baltimore, MD: The Johns Hopkins Press, 1989.

[54] T. Dhaene, L. Martens, and D. Dezutter, "Adaptive frequency sampling algorithm for fast and accurate *S*-parameter modeling of general planar structures," in *IEEE MTT-S Int. Microwave Symp. Dig.,* Orlando, FL, May 1995, pp. 1427-1430.

[55] J. Umoto and T. Hara, "A new digital analysis of surge performance in electric power networks utilizing the convolution integral," *Journal of the Institute of Electrical Engineers in Japan*, vol. 91, no. 3, pp. 48-57, 1971.

[56] A. Semlyen and A. Dabuleanu, "Fast and accurate switching transient calculations on transmission lines with ground return using recursive convolution, " *IEEE Trans. Power Apparatus and Syst.,* vol. PAS-94, no.2, pp. 561-571, March/April 1975.

[57] T. Hu, B. Zhong, S. L. Dvorak, and J. L. Prince, "Application of recursive convolution to transient simulation of interconnects using a hybrid phase-pole macromodel," *IEEE Trans. Advanced Packaging*, vol. 27, no. 4, pp. 603-610, November 2004.

[58] W. S. Cleveland, "LOWESS: A program for smoothing scatterplots by robust locally weighted regression," *The American Statistician*, vol. 35, pp. 54, 1981.

[59] W. S. Cleveland, "Robust locally weighted regression and smoothing scatter plots," *J. Amer. Statist. Assoc.* vol. 74, pp. 829–836, 1979.

[60] D. Saraswat, R. Achar, and M. Nakhla, "Restoration of passivity in S-parameter data of microwave measurements," *Proc. IEEE International Microwave Symposium*, Long Beach, CA, June 2005.

[61] D. Pozar, *Microwave Engineering.* Reading, MA: Wiley, 1993.

[62] G. W. Stewart and J.-G. Sun, *Matrix Perturbation Theory.* Boston: Academic Press, 1990.

[63] R. Mandrekar and M. Swaminathan, "Causality enforcement in transient simulation of passive networks through delay extraction," in *Proceedings of the 9th IEEE Workshop on Signal Propagation on Interconnects,* Germany, May 10-13, 2005, pp 25-28.

[64] F. M. Tesche, "On the use of the Hilbert transform for processing measured CW data," *IEEE Transactions on Electromagnetic Compatibility*, vol. 34, no. 3, pp. 259-266, Aug. 1992.

[65] T. R. Arabi and R. Suarez-Gartner, "Time domain analysis of lossy multi-conductor transmission lines using the Hilbert transform," *IEEE MTT-S International Microwave Symposium Digest*, vol.2, pp. 987-990, June, 1993.

# AUTHOR'S BIOGRAPHY

Rong Gao received the B.E. and M.S. degrees in electrical engineering from the Northwestern Polytechnical University, Xi'an, P.R. China, in 1995 and 1998, respectively. She is currently working toward the Ph.D. degree at the University of Illinois at Urbana-Champaign.

Since 2001, she has been a research assistant in the Department of Electrical and Computer Engineering, University of Illinois at Urbana-Champaign. Her current research interests include efficient macromodels for high-speed interconnect structures, fast algorithms for large-scale circuit simulation, and signal integrity.